Applied Energy 413 (2026) 127776

Contents lists available at ScienceDirect

Applied Energy

journal homepage: www.elsevier.com/locate/apenergy

Advanced national Atlas and Export outlook of green hydrogen: The Algerian case

Mawloud Guermoui [a,b,*], Abdelfetah Belaid [b], Farid Melgani [a]

[a] Department of Information Engineering and Computer Science, University of Trento, via Sommarive, n. 9, Trento 38123, Italy

[b] Unité de Recherche Appliquée en Energies Renouvelables, URAER, Centre de Développement des Energies Renouvelables, CDER, Ghardaïa, Algeria

HIGHLIGHTS

- High-resolution photovoltaic and hydrogen potential maps for Algeria are developed.
- Grid, corridor, and off-grid siting constraints quantify deployable land availability.
- Cost maps identify competitive hydrogen zones at about 4.6–5.2 euros per kilogram.
- Environmental maps quantify carbon dioxide and natural gas displacement potential.
- Export pathways of 10 million tonnes per year assess land and water requirements.

ARTICLE INFO

Keywords:
Green hydrogen
Spatial analysis
PV driven electrolysis
Scenario analysis
Techno economic assessment
Decarbonization

ABSTRACT

Algeria combines exceptional solar resources with emerging European demand for low carbon molecules, positioning the country as a strategic candidate for large scale green hydrogen. This study develops a spatial decision support framework that links a national photovoltaic direct current yield **(PV DC yield)** atlas to a hydrogen production atlas, techno economic evaluation, and screening level environmental co benefits. Two PV configurations, horizontal and optimally tilted are assessed on a land normalized basis and converted to hydrogen production. To reflect deployment realism, the analysis applies multiple infrastructure and accessibility scenarios that differentiate feasible development envelopes. In addition, an export oriented outlook is examined to assess how Algeria could contribute up to 10 million tons of hydrogen per year (**10 Mt $H_2 \cdot yr^{-1}$**) to European markets through alternative pathways, including pipeline based delivery, desalination supported water supply, and electricity export concepts, with explicit attention to water availability and sourcing. The maps reveal strong geographic gradients in PV productivity that propagate into hydrogen density and cost competitiveness. Optimal tilt systematically increases PV yield and hydrogen production density and reduces levelized cost of hydrogen (**LCOH**) across the territory, while scenario filters primarily reshape the reachable portfolio of low cost sites rather than the physics based ranking. For the modeled assumptions, LCOH spans approximately **4.6–5.2 €/kg H_2**, with tilted PV delivering a consistent cost improvement relative to horizontal PV. Environmental indicators indicate substantial benefits versus grey hydrogen, with avoided CO_2 and natural gas displacement concentrating in the highest productivity zones. Overall, the atlas results provide an integrated

Abbreviation: AC, Alternating current; AEC, Alkaline Electrolyzer cell; AEP, Annual energy production; BOP, Balance of plant; CAPEX, Capital expenditure; CF, Capacity factor; CO_2, Carbon dioxide; CSP, Concentrated solar power; DC, Direct current; DC/DC, Direct-current to direct-current converter; DHI, Diffuse horizontal irradiance; DNI, Direct normal irradiance; EL, Electrolyser; EPC, Engineering, procurement, and construction; EU, European Union; FC, Fuel cell; FCR, Fixed charge rate; GHG, Greenhouse gas; GHI, Global horizontal irradiance; GIS, Geographic information system; GTI, Global tilted irradiance (plane-of-array irradiance); HHV, Higher heating value; H_2, Hydrogen; HVDC, High-voltage direct current; IEA, International Energy Agency; IRR, Internal rate of return; kWh, Kilowatt-hour; kW, Kilowatt; LCA, Life-cycle assessment; LCOE, Levelized cost of electricity; LCOH, Levelized cost of hydrogen; m^3, Cubic meter; MoU, Memorandum of understanding; NG, Natural gas; NWSAS, North Western Sahara Aquifer System; O&M, Operations and maintenance; OPEX, Operating expenditure; PEM, Proton exchange membrane; POA, Plane-of-array; Pt.X, Power-to-X; PV, Photovoltaic; RO, Reverse osmosis; SAPM, Sandia Array Performance Model; SMR, Steam methane reforming; STC, Standard test conditions; TSO, Transmission system operator; WACC, Weighted average cost of capital.

* Corresponding author at: Department of Information Engineering and Computer Science, University of Trento, Italy.
E-mail address: mawloud.guermoui@unitn.it (M. Guermoui).

https://doi.org/10.1016/j.apenergy.2026.127776
Received 19 January 2026; Received in revised form 18 March 2026; Accepted 22 March 2026
Available online 30 March 2026

evidence base to prioritize investment corridors, quantify trade-offs between resource quality and infrastructure access, and support export scale planning with water supply and electricity matching considerations.

1. Introduction

Hydrogen is increasingly positioned as a pivotal option for decarbonizing "hard to abate" activities where direct electrification is technically constrained or cost prohibitive, including heavy industries (e.g., steelmaking and chemical production), high temperature process heat, and energy intensive transport modes such as heavy duty vehicles, shipping, and aviation [1]. In net zero pathways, multiple outlooks converge on a major scale up of hydrogen and its derivatives by mid-century; for instance, the Hydrogen Council estimates that achieving a net-zero trajectory could require on the order of 660 Mt. of renewable and low-carbon hydrogen use in 2050, corresponding to roughly 22% of projected global final energy demand in 2050 [2].

Because hydrogen's **climate mitigation benefit** depends primarily on its **greenhouse-gas intensity** (which is determined by the production pathway), it is commonly classified by carbpon-intensity categories. For example, grey hydrogen is produced from fossil fuels typically natural gas via steam methane reforming without carbon capture, and is therefore associated with substantial greenhouse-gas emissions [3], with high carbon footprint, commonly reported around 9–12 kg.CO_2 per kg. H_2 [4]. Blue hydrogen refers to fossil based hydrogen produced with carbon capture, utilization and storage (CCUS), which can reduce though not necessarily eliminate emissions depending on capture performance and upstream supply chain emissions. Purple hydrogen is produced using nuclear electricity (often via electrolysis), and green hydrogen is generated by water electrolysis powered by renewable electricity, yielding very low operational emissions when the electricity is demonstrably renewable [5]. The IEA reports that global hydrogen production reached almost 100 Mt. in 2024, reflecting total output across all routes and still dominated by fossil based production rather than renewable hydrogen. Low emissions hydrogen from low carbon electrolysis and/or fossil production with CCUS accounted for <1% of supply, underscoring the limited penetration of low emissions pathways [6,7]. Consistent with this supply mix, the IEA reports that hydrogen production emitted ~920 Mt.CO_2 in 2023, largely driven by unabated natural gas and coal routes [7].

Within the broader energy transition agenda shaped by international climate agreements, such as the Kyoto Protocol (adopted 1997; entered into force 2005) [8],and the Paris Agreement decarbonization strategies prioritize direct electrification wherever feasible [9], enabled by the maturity and rapidly improving economics of renewable power (notably wind and solar).

In this context, Algeria is well positioned to participate in the emerging low emission hydrogen economy. Building on exceptional solar resources and large developable land areas already demonstrated through high resolution PV suitability and performance assessments [10]. Algeria has begun formalizing hydrogen governance and international cooperation. Notably, the national hydrogen development strategy was published by the Renewable Energy and Energy Efficiency Commission (CEREFE) in February 2024 [11], and Algeria and Germany established a bilateral hydrogen taskforce alongside plans for a green hydrogen pilot plant. In parallel, the EU–Germany co financed TaqatHy+ program aims to accelerate renewable deployment, develop the green hydrogen value chain, and strengthen energy efficiency measures in Algeria [12].

Crucially, Algeria's opportunity is reinforced by a clear external demand signal from Europe. The EU's REPowerEU plan sets an indicative target of 10 Mt./year of domestic renewable hydrogen production and 10 Mt./year of renewable hydrogen imports by 2030 [13], and EU mechanisms such as the European Hydrogen Bank are designed to help bridge early market cost gaps and support scalable deployment. Infrastructure concepts are also advancing, including the SoutH2 / Southern Hydrogen Corridor connecting North Africa with Italy, Austria, and Germany supported through EU cross border infrastructure prioritization and political declarations among participating countries [14].

This policy and market landscape motivates a structured transition logic of electrification first, and molecules where necessary. In practice, solar PV expansion supports rapid power-sector decarbonization and end-use electrification, while residual emissions in hard-to-abate sectors can be addressed via PV-powered green hydrogen and downstream **Power-to-X (Pt.X)** pathways (e.g., hydrogen-to-ammonia for fertilizers and maritime fuels, and other synthetic fuels for aviation and shipping). Against this backdrop, translating Algeria's PV performance and siting advantages into a spatially explicit **PV-powered Pt.X planning framework** inking PV deployment zoning to hydrogen production and downstream Pt.X options while accounting for realistic infrastructure, water sourcing, and delivery corridors becomes essential for investment-grade screening and strategic energy planning.

Accordingly, this study advances prior Algeria-focused assessments by presenting an end-to-end, deployment-grade national PV-to-hydrogen (H_2) production planning workflow that explicitly distinguishes technical potential from deployable potential under infrastructure and water constraints. The main contribution is the integration of established modelling components into a single spatial decision-support chain that links PV zoning, H_2 production, techno-economic performance, and export-scale feasibility. Specifically, the framework delivers:

Multi scenario hydrogen siting logic A hydrogen oriented site suitability workflow under three complementary development logics **grid connected deployment,** a **north–south grid corridor scenario** to mitigate Algeria's resource–demand mismatch, and an **offline (remote) scenario** that reveals intrinsically favorable areas independent of current infrastructure.

PV–DC production atlas (two configurations) A national PV–DC production atlas for **horizontal** and **optimally tilted** systems, informed by and calibrated against performance characteristics of a representative **grid connected PV plant.**

1. **National hydrogen production atlas** Spatial conversion of PV yield into a national **hydrogen production atlas** for both PV configurations across all development scenarios.

Spatially explicit LCOH mapping Territory wide **levelized cost of hydrogen (LCOH)** maps, explicitly incorporating **scenario dependent access and connection cost adders** to reflect realistic deployment conditions.

Environmental co benefits screening Quantification of screening level environmental benefits, including **avoided CO_2 emissions and indicative natural gas displacement,** benchmarked against conventional **grey hydrogen** pathways.

- **Export outlook for Europe (10 Mt $H_2 \cdot yr^{-1}$)** A scenario based export assessment that explores pathways for supplying **10 Mt $H_2 \cdot yr^{-1}$** from Algeria to Europe primarily via **pipeline delivery** and contrasts alternative **electrolysis make-up water** sourcing strategies (groundwater-based hubs versus seawater desalination supported supply), providing first-order land and **electrolysis water** requirements to inform export-scale feasibility.

The rest of the paper is organized as follows. Section 2 reviews related work and identifies the research gap. Section 3 describes the materials, datasets, and overall methodology. Section 4 presents the spatio-temporal PV DC production modelling and the national PV atlas generation. Section 5 details the PV DC–driven electrolysis model for hydrogen production (HHV basis). Section 6 introduces the techno-economic assessment and the environmental performance metrics. Section 7 reports the main results and their interpretation. Section 8 discusses export-oriented production scenarios and the Algeria–Europe outlook. Section 9 addresses the generalizability and transferability of the framework. Section 10 concludes with key findings and implications.

2. Related work and research gap

Recent research on spatial planning for green hydrogen can be organized into four complementary streams: (i) techno-economic hydrogen atlases, (ii) GIS suitability/MCDM siting, (iii) export-corridor and infrastructure optimization, and (iv) governance and water-constraint readiness. Collectively, these studies show rapid progress in mapping hydrogen potential and costs, but they also reveal a persistent integration gap: few frameworks simultaneously combine land-eligible deployable potential, scenario-conditioned infrastructure feasibility, water sourcing constraints, and export-scale corridor logic within a unified national decision-support workflow.

National and regional hydrogen atlases increasingly couple high-resolution solar/wind data with electrolysis modelling to generate spatial layers of hydrogen yield/density, LCOH, and CO_2 mitigation [15–19]. These studies consistently identify low-cost hotspots driven by superior renewable regimes: for example, Brazil's northeast emerges as the most competitive region, with reported minimum LCOH values around 2.35 \$/kg (solar) and 3.44 \$/kg (wind) under the study assumptions [15]. For Egypt, atlas mapping under PV–wind land-sharing scenarios reports hydrogen production densities up to 5.71 kg/m^2 and minimum LCOH values down to 1.02 \$/kg in wind-dominated coastal regions [17]. Wind-only atlas work for Portugal reports minimum $LCOH_2$ around 3.26 €/kg in high-resource locations [18]. More comprehensive cost-mapping at province level in China integrates land suitability and water availability and projects substantial spatial cost dispersion, with 2030 LCOH as low as ~ 1.44 \$/kg in inland provinces and above ~ 4.5 \$/kg in coastal provinces under policy and tariff differentiation [18]. Beyond PV–electrolysis, geospatial assessments have also extended to alternative hydrogen pathways; for instance, Li et al. (2025) [19] combine land suitability constraints with meteorological variability and machine-learning optimization to estimate a national-scale hydrogen potential of ~216.6 Mt. for solar photocatalysis, benchmarking against PV–electrolysis and highlighting the importance of temporal dynamics for storage and downstream conversion. Despite strong resource and cost cartography, many atlas studies still evaluate PV and wind independently and often omit or simplify the spatial layers that determine deploy ability at scale particularly land-use eligibility, grid/pipeline conditioning, export-scale targets, and explicit water sourcing constraints [15]– [17]. As a result, they can identify where hydrogen is cheap in principle but not necessarily where it is feasible and exportable under real infrastructure and water constraints.

A second stream uses GIS–MCDM methods (AHP, fuzzy-AHP, ANP-weighted overlays, TOPSIS/VIKOR/PROMETHEE variants) to classify territories into suitability classes based on resource intensity, slope/elevation, exclusions, proximity to infrastructure, and often water access [21–24]. These studies provide decision-support outputs that are practical for early-stage site screening. Some also report techno-economic values for selected sites, such as a regional Moroccan assessment that estimated LCOH around 2.9 \$/kg for a selected PV-based configuration [20], and a site-scale Moroccan hybrid evaluation reporting LCOH around 3.10–3.27 \$/kg depending on configuration and reliability trade-offs [24]. Provincial work in Iran embeds HOMER-derived economic indicators directly into GIS suitability mapping and reports LCOH in the 3.6–5.1 \$/kg range for a fixed demand case [25]. Earlier province-scale GIS-based techno-economic mapping also illustrates the foundations and limitations of this approach; for example, Nematollahi et al. (2019) [26] interpolate measured wind/solar resources to map hydrogen production potential and generation costs at provincial level, but without national land filtering, water constraints, or corridor-scale infrastructure integration. Many suitability studies prioritize ordinal suitability classification over consistent national-scale land-normalized hydrogen density and spatial LCOH maps, and they rarely connect suitable zones to export deliverability (pipelines/ports) or large-scale production targets. Thus, they support “where could we build?” more than “how much could we export competitively, and through which corridors?”

A third, fast-growing body of work treats hydrogen as a supply-chain commodity requiring hubs, logistics, and corridor design. For Türkiye, a multi-hub off-grid framework identifies production hubs via clustering and facility location methods and connects them to an export port through pipeline network design, reporting a delivered total LCOH of ~ 6.83 USD/kg under full utilization assumptions and exploring competitiveness via subsidy scenarios [27]. In China, national optimization models combine GIS-based pipeline routing (least-cost pathfinding) with inter-provincial dispatch and show that integrating pipeline transmission with power-grid options can reduce total system costs by ~ 15% versus single-mode designs [28]. Brazil cluster analysis further highlights spatial mismatch between production-rich areas and demand centers, motivating corridor development and transmission planning [29].These models advance delivered-cost and network realism, but they are not always anchored to a consistent resource-to-hydrogen atlas and often lack integrated treatment of land eligibility, water sourcing, and renewable variability within the same framework. This separation keeps “atlas mapping” and “corridor design” as parallel literatures rather than a unified national planning workflow.

Finally, foresight and stakeholder studies emphasize that institutional capacity, social acceptance, and water scarcity can dominate implementation outcomes. Scenario-based foresight for Kenya identifies societal acceptance and infrastructure robustness as key drivers shaping adoption trajectories [30], while stakeholder surveys in Jordan highlight intermittency, limited pipelines/storage, high LCOH, and water scarcity as major constraints, with desalination frequently cited as a mitigation option [31].

While crucial for implementation realism, these studies typically do not quantify spatial production density or cost surfaces, nor do they integrate water constraints into spatial techno-economic planning outputs.

Compared with the international literature above, Algeria-specific spatial research remains relatively sparse and largely resource-oriented. Early national assessments map solar/wind-to-hydrogen potential per area and identify promising southern zones, but do not include scenario-based infrastructure feasibility, export targets, water sourcing, or spatial LCOH [32]. PV-driven simulation work provides national maps of hydrogen yield and optimal tilt, yet does not address grid/off-grid development logics, export corridors, or water sourcing feasibility [33]. Site-based analyses evaluate PV–Electrolyzer–fuel cell concepts for representative locations but do not provide deployable national atlas outputs with land exclusions, water feasibility, and export logistics [34]. More recent national GIS assessments incorporate infrastructure mainly through proximity buffers, with limited on-grid/off-grid scenario differentiation and without explicit water sourcing and export corridor scenarios [35].

In summary, recent international research has advanced spatial hydrogen planning through techno-economic hydrogen atlases that map renewable-to-hydrogen potential and LCOH hotspots, GIS-based multi-criteria suitability screening, and export- and infrastructure-oriented corridor modelling. However, these strands are often developed separately, and few studies integrate within one national workflow **deployable land-normalized potential, scenario-conditioned infrastructure feasibility, explicit water sourcing constraints,** and an **export-scale stress test.** This integration gap is particularly pronounced for Algeria, where spatial studies remain limited and largely

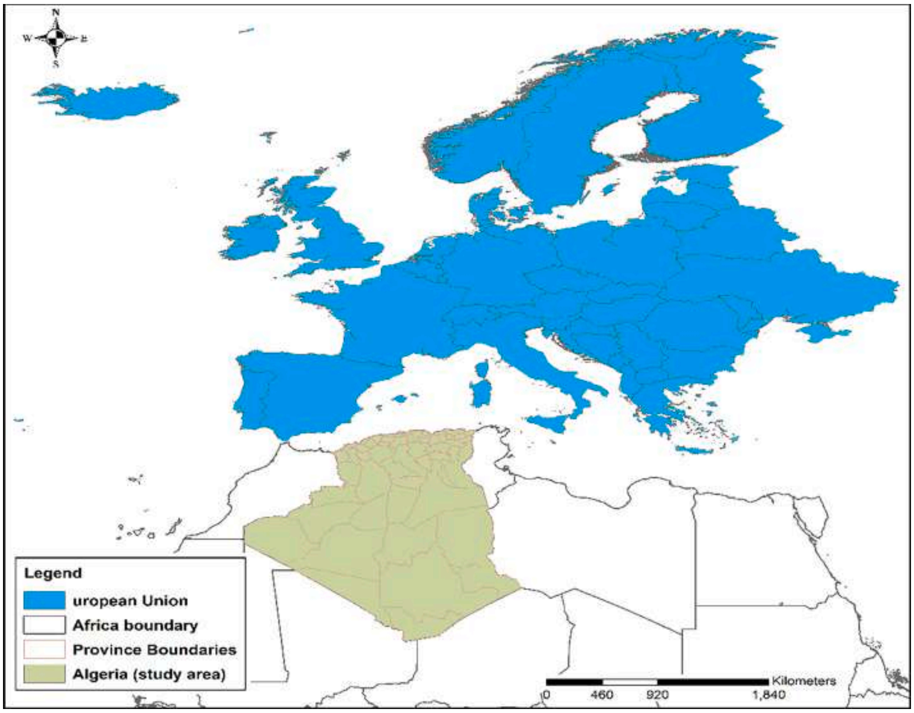

Fig. 1. Study area and regional context.

fragmented.

To address this gap, the present study implements an end-to-end PV-to-hydrogen decision-support workflow that links eligibility masking, PV DC yield modelling, hydrogen density and LCOH mapping, and export-scale land–water implications. The following section details the data, assumptions, and methodology used to develop the national atlas and the associated scenario analyses.

3. Materials and methods

3.1. Study area and data

Algeria is **Africa's largest country,** with an approximate surface area of 2.38 million km^2 (see Fig. 1), **80%** of its territory located in the **Sahara Desert,** offering continental-scale land availability within one of the world's **highest solar-irradiation (high-insolation) belts** [36]. Long term solar resource layers (e.g., Global Solar Atlas) indicate a strong north–south gradient, with average **GHI** $\approx$ **4.6–6.6 kWh/m^2/day** from the Mediterranean north to the Saharan south, and sunshine duration reaching **up to 3500 h/year** in high insolation regions [37]. Its **Mediterranean coastline** faces directly toward Europe, reinforcing the strategic relevance of cross border low carbon energy linkages; notably, in **2024** Sonatrach and Sonelgaz signed an MoU with **ENI** to study a **subsea Algeria–Italy power interconnection**, explicitly framed around future low carbon exchanges [38].

From a policy perspective, Algeria's National Program for the Development of Renewable Energies targets 15,000 MW by 2035, aiming for roughly a 30% renewable share in electricity. Within this trajectory, solar PV is expected to dominate, with around 13.5 GW planned by 2030. Recent announcements further indicate that the first ~3.2 GW tranche of utility scale solar is scheduled to enter operation starting from 2025 [38–39]**,** providing near term momentum for grid connected PV expansion and, by extension, early PV to green hydrogen hub development.

3.2. Methodological workflow and modelling blocks

The methodological pipeline follows a sequential logic that links geospatial eligibility screening, PV energy modelling, and PV to hydrogen conversion into a consistent national mapping framework. As illustrated in the workflow (Fig. 2), the approach is organized into **three main blocks (Block 1)** *PV–H$_2$ geodatabase construction and scenario/ eligibility masking* (criteria compilation, GIS harmonization, and Boolean restriction maps); **(Block 2)** *Spatio-temporal PV production modelling and spatial PV atlas generation* using SAPM[1] for **horizontal** and **optimally tilted** configurations; and **(Block 3)** *hydrogen chain assessment* that converts PV DC electricity to Electrolyzer input and produces the downstream atlases of **hydrogen production density, LCOH, and environmental indicators**, under the defined development scenarios.

3.3. Block 1 PV–H$_2$ geodatabase and evaluation logic

Prior to PV yield modelling and PV-to-hydrogen conversion, a national eligibility **screening** is applied using GIS-based exclusion masks and compatibility buffers (Table 1) to delineate land suitable for PV–Electrolyzer hub deployment. In this study, the screening layers are organized according to the common siting categories reported in Table 1 (environmental, climatic/resource, topographical/technical, and economic/infrastructure constraints). The **legal** dimension is not represented as a standalone spatial layer; instead, it is captured implicitly through mapped protection status and land-use restriction proxies embedded in the exclusion layers (e.g., protected areas and restricted/ controlled zones such as settlements and safety buffers, airports, military areas, petroleum regions, and quarries). Accordingly, the screening removes: (i) protected and ecologically sensitive areas and hydrological constraints, (ii) incompatible or restricted land uses and buffer-based exclusion zones, and (iii) technically/geotechnically unsuitable terrain (e.g., steep slopes, high elevation limits, dunes and moving sands).

[1] https://pvpmc.sandia.gov/modeling-guide/2-dc-module-iv/point-value-models/sandia-pv-array-performance-model/

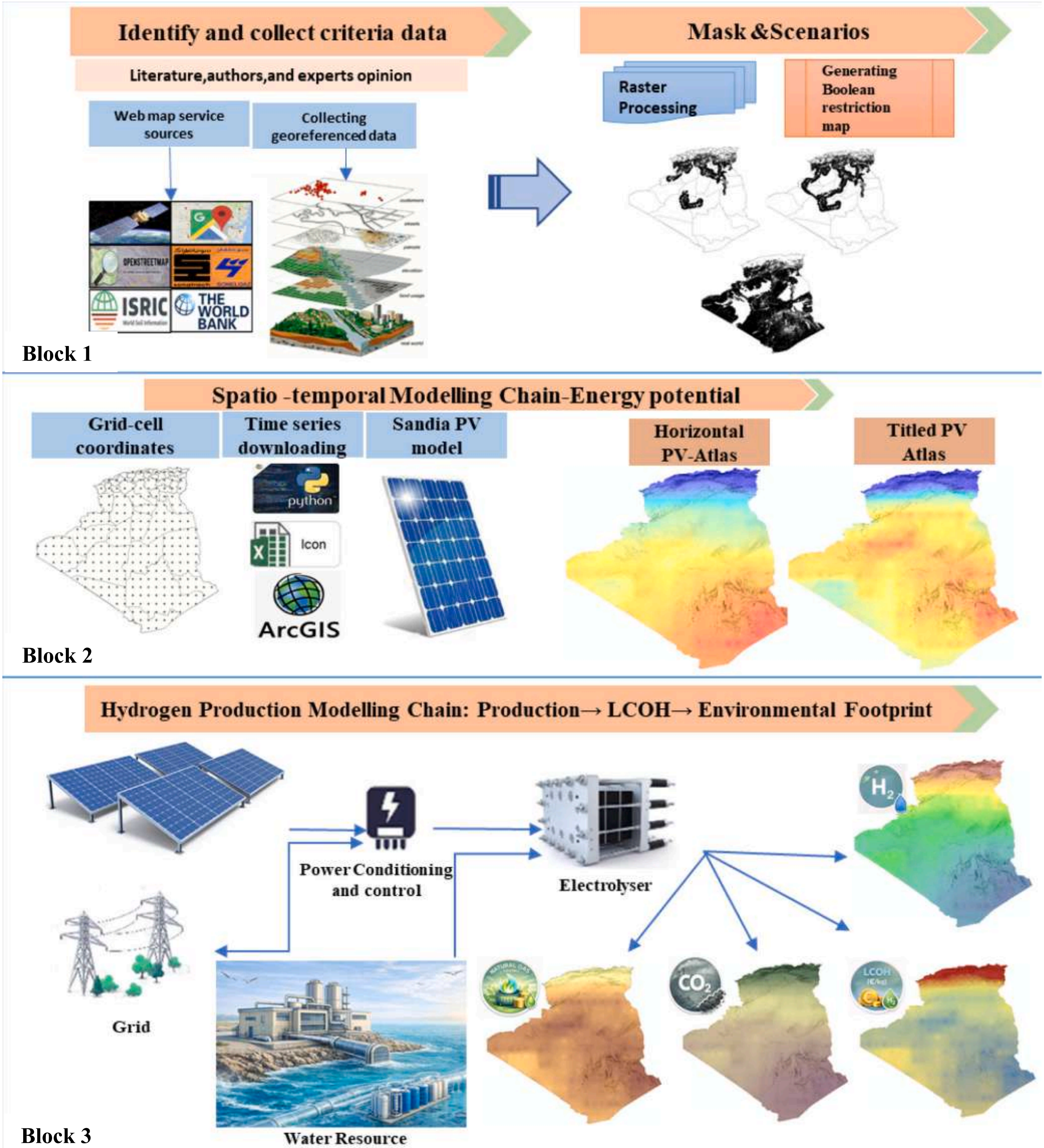

Fig. 2. Methodological flowchart for PV resource mapping, scenario masking, and PV-to-hydrogen assessment.

Additional proximity-based setbacks (i.e., minimum separation distances implemented as buffer-based exclusion zones) are applied around safety- and security-relevant features (e.g., airports and restricted sites) and around settlements to reduce land-use conflicts. Infrastructure layers (grid, roads, settlements) are used here strictly to enforce practical constructability and access constraints; the PV production atlas and subsequent hydrogen production and LCOH mapping are introduced later under the defined development scenarios.

The eligibility masks show that enforceable infrastructure constraints strongly shape the deployable land envelope for PV–Electrolyzer hubs. Under the **existing transmission-grid baseline**, only **13.68%** of Algeria remains viable, which increases modestly to **15.91%** with the **north–south corridor** scenario, while the **infrastructure independent (offline)** case expands viable deployment to **71.35%,** because grid- and access-related constraints (proximity to transmission lines, roads, and settlement) are relaxed, leaving only the infrastructure-independent eligibility filters (e.g., protected areas/water bodies and topographic/geotechnical exclusions) to constrain siting

Table 1
PV–H_2 eligibility screen datasets and exclusion/buffer rules used to delineate deployable land for PV–Electrolyzer hubs ('–' denotes not reported by the data source).

Category	Criteria	Type (Format)	Data period	Scale/ resolution	Source	Restrictions /Buffer	References
Environment	Natural Protected Areas, Regional Conservation Areas, Private Conservation Areas, Permanent Production Forests.	Vector –polygon shapefile	2023	–	Geofabrik (OSM Algeria extract): https://download.geofabrik.de/africa/algeria.html	No less than 1000 m	[41–47]
	Water bodies	Vector –polygon shapefile	2024	–	Esri Living Atlas (Land Cover Explorer): https://livingatlas.arcgis.com/landcoverexplorer	No less than 1000 m	[41 –48]
	Wetlands	Vector –polygon shapefile	2024		Esri Living Atlas (Land Cover Explorer): https://livingatlas.arcgis.com/landcoverexplorer	No less than 1000 m	[41,43,45–48]
	Soil Type	Raster	1995–2019	1 × 1 km	FAO soils portal (HWSD v2.0): https://www.fao.org/soils-portal/data-hub/soil-maps-and-databases/harmonized-world-soil-database-v20/en/	dunes and moving sand excluded	Expert
	Petroleum regions	Vector – point shapefile	2024	–	OpenStreetMap (OSM) https://www.openstreetmap.org/	No less than 1500 m	Expert
	Military areas	Vector – point shapefile	2024	–		No less than 1500 m	Expert
	Quarries	Vector –polygon shapefile	2024	–		No less than 2000 m	Expert
	Airports	Vector – point shapefile	2024	–		No less than 1500 m	
Climatic	Global Horizontal irradiation.	Raster	1994–2018	250 × 250 m	Global Solar Atlas https://globalsolaratlas.info/map	No less than 1300 Kwh/m^2	[41,49,50]
Topographical	Elevation	Raster	2000	30 × 30 m	USGS EarthExplorer https://earthexplorer.usgs.gov/	No more than 1.5 km	[41,48]
	Slope	Raster	2000	30 × 30 m		No more than 11%	[41,44,47]
Economic	Power transmission lines	Vector –lines shapefile	–	–	Official government data (Algeria transmission network / Sonelgaz)	Exclusion buffer of 100 m from both sides; sites >50 km from line are excluded.	[41,43,44,48]
	Major Road	Vector –lines shapefile	–	–	OpenStreetMap (OSM) https://www.openstreetmap.org/	Exclusion buffer of 500 m from both sides; sites >50 km from line are excluded.	[41,45,48]
	Distance to settlement areas (m)	Raster	2024	30 × 30 m	Esri Living Atlas (Land Cover Explorer / settlement layer, 2024) https://livingatlas.arcgis.com/landcoverexplorer/	Exclusion buffer of 1 km from both sides; sites >50 km from line are excluded.	[41,44,48,51]

Note: "No less than" indicates a *minimum setback (buffer) distance*.

(Fig. 3).

Block 2 Sandia Array Performance Model (SAPM) Driven PV Production Modelling and Spatial PV Atlas Generation.

This subsection describes the PV power production modelling adopted to generate national PV DC atlases for two configurations (i) horizontal PV (tilt = 0°) and (ii) optimally tilted PV. The workflow converts gridded (**100 km × 100 km spatial resolution; hourly 2019 data)**,meteorological and radiation time series (irradiance components, ambient temperature, wind speed, and surface albedo) into hourly DC power, which is then aggregated to annual/seasonal PV yield layers suitable for subsequent PV–H_2 conversion.

To generate the photovoltaic (PV) production atlas over Algeria for horizontal PV ($\beta = 0°$) and optimally tilted PV ($\beta = \beta^*$), we compute the Global Tilted Irradiance (GTI) from gridded radiometric inputs and solar geometry. The radiometric database[2] provides global horizontal irradiance (GHI) and diffuse horizontal irradiance (DHI), together with surface albedo (ρ). Solar position (solar altitude and incidence angles) is derived from latitude/longitude, day of year, and solar time.

Block 3 Hydrogen production atlas from the PV DC atlas.

This subsection converts the land-normalized PV DC atlas (Section 2.3.3) into a spatially explicit hydrogen production atlas over Algeria. The PV-to-hydrogen conversion is first performed on the **native input grid (100 km × 100 km)** for both PV configurations (horizontal PV and optimally tilted PV). The resulting PV and hydrogen atlas layers are then **interpolated/resampled to 100 m × 100 m** resolution to produce refined national-scale maps for the subsequent spatial analyses. **Because. PV output has already been scaled to a realistic 1 km^2 parcel with 34% PV occupation, the resulting hydrogen atlas represents deployment grade (not theoretical) production potential [40].**

4. Spatio-temporal PV DC production modelling and national PV atlas generation

4.1. Plane of array irradiance using the Perez anisotropic sky model

At each time step, the beam horizontal irradiance (BHI) is obtained by subtracting diffuse from global horizontal irradiance [52].

$$BHI = GHI - DHI \tag{1}$$

The corresponding direct normal irradiance (DNI) is reconstructed

[2] https://power.larc.nasa.gov/

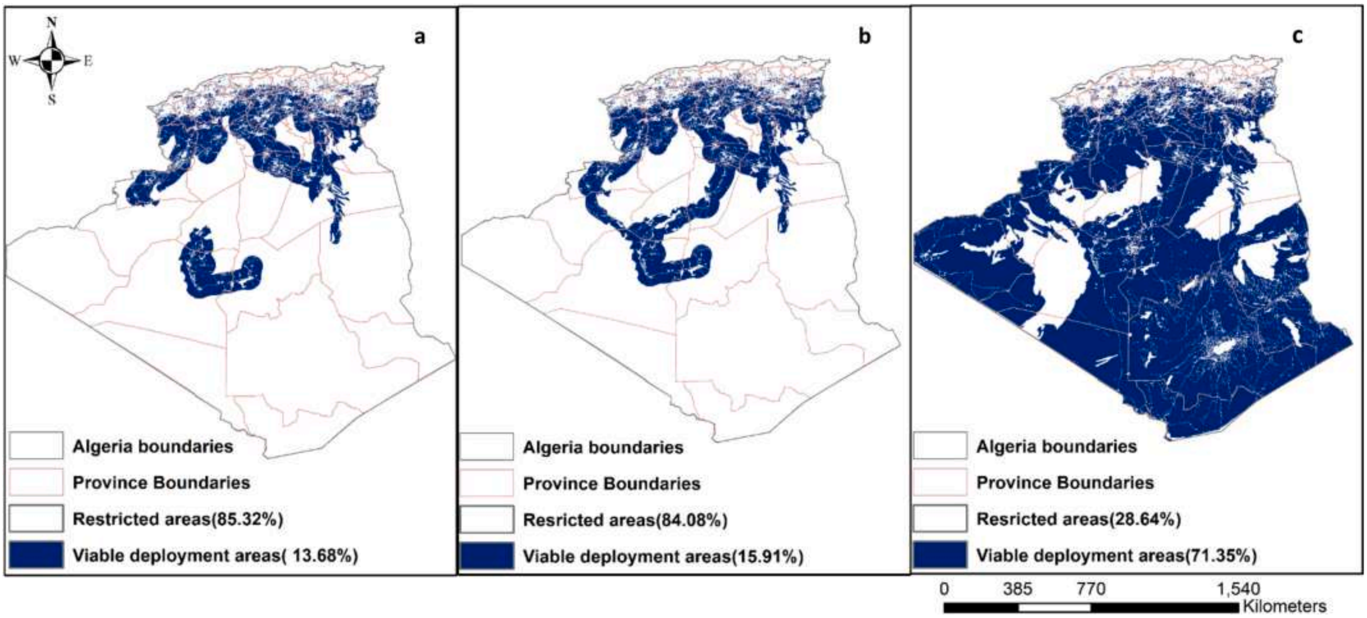

Fig. 3. Eligibility mask outcomes for PV–Electrolyzer hub deployment in Algeria under three infrastructure scenarios ***(a)*** grid connected baseline using the existing transmission network (reference case), ***(b)*** north–south grid corridor interconnection scenario, and ***(c)*** offline (infrastructure independent).

using the solar altitude angle α_s

$$DNI = BHI/\sin(\alpha_s) \tag{2}$$

The beam component on the tilted plane is then

$$G_{b,\beta} = DNI\cos(\theta) \tag{3}$$

Diffuse irradiance $G_{d,\beta}$ on an inclined plane is computed using the Perez anisotropic transposition model, which represents diffuse radiation as the sum of an isotropic background, a circumsolar component around the sun, and horizon brightening.

$$G_{d,\beta} = DHI\left[(1-F_1)\frac{1^{*}\cos\beta}{2} + F_1\left(\frac{a_1}{a_2}\right) + F_2\sin\beta\right] \tag{4}$$

The geometry terms are defined as [52].

where F_1 and F_2 are the Perez circumsolar and horizon brightening coefficients, respectively. The geometry terms are

$$a_1 = \max(0, \cos\theta), a_2 = max(\cos 85^o, \sin\alpha_s)$$

where β is the tilt (slope) angle of the PV plane measured from the horizontal, and θ is the incidence angle of the sun on the tilted plane, i.e., the angle between the solar beam and the surface normal.

The ground reflected irradiance incident on the tilted plane is computed using a view factor approximation and the ground reflectance (albedo) ρ.

The grounded reflected irradiance incidence on the titled plane is computed as

$$G_{r,\beta} = GHI\left(\frac{1-\cos\beta}{2}\right)\rho \tag{5}$$

The global plane of array irradiance (GTI) is the sum of beam, sky diffuse, and ground reflected contributions

$$GTI(\beta) = G_{b,\beta} + G_{d,\beta} + G_{r,\beta} \tag{6}$$

4.2. SAPM based PV DC power modelling

After computing plane of array (POA/$GTI_\beta(t)$) irradiance for horizontal and optimally tilted surfaces using the Perez anisotropic sky model, PV module DC output is estimated at each grid cell using the Sandia Array Performance Model (SAPM) [53]. SAPM couples horizontal and optimally tilted surfaces irradiance with key meteorological drivers (notably ambient temperature and wind speed) to predict module operating temperature and the corresponding electrical performance, thereby enabling spatially consistent PV DC atlases for (i) horizontal and (ii) optimally tilted PV configurations.

We parameterize the module using the Sandia PV module database entry "SunPower_SPR_220_BLK_U_Module_2008_E_" (rated at 221.38 W under standard test conditions, STC; aperture area **1.244 m²**). The SAPM coefficients provided for this module include the reference I—V points (Isc0, Imp0, Voc0, Vmp0), temperature coefficients (αIsc, αImp, βVoc, βVmp), and empirical correction factors for spectral effects and angle of incidence response.

(a) Module and cell temperature.

Module operating temperature is estimated from ambient conditions using the Sandia temperature model, in which the back surface module temperature is a function of $GTI_\beta(t)$ irradiance,air temperature and wind speed. The cell temperature is then obtained from the module temperature [53,54].

$$T_m = T_a(t) + GTI_\beta(t)\ exp(a + b.WS(t)) \tag{7}$$

Cell temperature is then obtained from module temperature using an empirical temperature rise coefficient

$$T_c(t) = T_m(t) + \left(\frac{GTI_\beta(t)}{E_0}\right) + \Delta T \tag{8}$$

Here T_a is ambient air temperature (°C), WS is wind speed (m·s^{-1}), POA is irradiance (W·m^{-2}), E_0 = 1000 W·m^{-2}, Tm is module back surface temperature (°C), and Tc is cell temperature (°C). The coefficients a, b, and ΔT depend on the mounting configuration (e.g., open rack vs. close mounted) and are taken from the SAPM temperature parameter set.

(b) Effective irradiance (SAPM electrical driver).

SAPM transforms the physical irradiance on the module plane into an effective irradiance E_e, accounting for spectral mismatch (air mass effects), angle of incidence (AOI) losses, and the reduced module response to diffuse light. For a given time step [55].

$$E_e(t) = \frac{f_1(AM_a(t))\left[E_{b,\beta}(t)f_2\ (AOI(t)) + f_d E_{d,\beta}(t)\right]}{E_0}\ SF \tag{9}$$

$E_{b,\beta}$ and $E_{d,\beta}$ are the beam and diffuse components, respectively; AOI is the solar incidence angle on the module plane (degrees); AM_a is absolute air mass; SF is a soiling factor (SF = 1 in this atlas study); and f_d is the diffuse fraction term specified in the Sandia module database.[3]

The spectral and AOI modifiers are expressed as low order polynomials [53].

$$f_1(AM_a) = a_0 + a_1AM_a + a_2AM_a^2 + a_3AM_a^3 + a_4AM_a^4 \tag{10}$$

$$f_2(AOI) = b_0 + b_1AOI + b_2AOI^2 + b_3AOI^3 + b_4AOI^4 + b_5AOI^5 \tag{11}$$

With coefficients $\{a_i\}$ and $\{b_i\}$ are module specific and are provided by the Sandia PV module database.

(c) SAPM electrical operating points and DC power.

Given effective irradiance E_e and cell temperature T_c, SAPM computes the I—V curve key points. Short circuit current and current at maximum power are

$$I_{sc} = I_{sc0}E_e[1 + \alpha_{Isc}(T_c - T_0)] \tag{12}$$

$$I_{mp} = I_{mp0}\left(C_0E_e + C_1E_e^2\right)[1 + \alpha_{Imp}(T_c - T_0)] \tag{13}$$

Open circuit voltage and voltage at maximum power are

$$V_{oc} = V_{oc0} + N_s\delta(T_c)\ln(E_e) + \beta_{Voc}(T_c - T_0) \tag{14}$$

$$V_{mp} = V_{mp0} + C_2N_s\delta(T_c)\ln(E_e) + C_3N_s[\delta(T_c)\ln(E_e)]^2 + \beta_{Vmp}(T_c - T_0) \tag{15}$$

$$\delta(T_c) = \left(\frac{nk}{q}\right)(T_c + 273.15) \tag{16}$$

In (12)–(16), the subscript "0" denotes reference values at the Sandia reference conditions (SRC), defined by $E_0 = 1000\ W\cdot m^{-2}$, $AM_a = 1.5$, AOI = 0°, and $T_c = T_0 = 25\ °C$. N_s is the number of cells in series. The parameter $\delta(T_c)$ is the cell thermal voltage, where n is the diode factor, k is Boltzmann's constant, and q is the elementary charge. C_0–C_3 are empirical module coefficients provided in the Sandia database, and α_{Isc}, α_{Imp}, β_{Voc}, β_{Vmp},are temperature coefficients.

Finally, the module DC power at the maximum power point (MPP) is [56].

$$P_{mp,DC} = I_{mp}V_{mp} \tag{17}$$

The meteorological inputs used in the SAPM/PV modelling chain include hourly GHI, DNI, DHI, ambient temperature, 10 m wind speed, and surface albedo; these variables are then used to derive plane of array irradiance (GTI), as well as cell temperatures fields that drive the PV DC yield atlas (Fig.4).

For each grid cell, eqs. (1)–(18) are evaluated using **hourly** meteorological and irradiance time series ($\Delta t = 1$ h) to obtain a DC power time series for both horizontal and optimally tilted PV configurations. These hourly time series are aggregated to annual energy yield ($kWh\cdot m^{-2}\cdot yr^{-1}$) and capacity factor metrics, then spatially interpolated to produce national PV DC atlases that feed the downstream PV–H_2 conversion.

4.3. Land area scaling for PV DC atlas

To make the PV atlas directly usable for spatial planning and PV–H2 conversion, SAPM outputs are expressed on a **land area basis** rather than as module level or per installed kWp values. Specifically, PV DC power is aggregated to a standardized **1 km^2 reference parcel** at each grid cell for both configurations **horizontal PV** and **optimally tilted PV.**

Importantly, utility scale PV plants do not convert the entire site area into active PV aperture area. A substantial share of land is required for inter row spacing (to limit shading losses), inverter/transformer pads, access roads, drainage corridors, and operational setbacks. To reflect real deployment conditions, this study adopts a PV occupation fraction of 34%, inferred from the layout characteristics of a representative grid connected PV plant.

This land based scaling is critical because many regional PV potential studies implicitly assume full land coverage, which can **systematically overestimate** achievable energy density and, by extension, downstream hydrogen potential. By enforcing a realistic occupation factor, the resulting PV atlas is **deployment grade** rather than purely theoretical it better represents what can be built on the ground under practical engineering constraints.

5. Hydrogen production modelling (PV DC–driven electrolysis, HHV basis)

This section converts the PV DC yield atlas into a spatially explicit hydrogen production atlas at the grid-cell level for both PV configurations (horizontal and optimally tilted). PV outputs are expressed on a land-area basis by scaling each cell to a standardized **1 km^2** reference parcel and applying a **PV land-occupation fraction of 0.34,** reflecting realistic utility-scale layout constraints (row spacing, access roads, inverter/transformer pads, and setbacks) derived from a representative grid-connected PV plant [54]. Hydrogen production is then computed using an Higher Heating Value HHV-based electrolysis representation, so the resulting maps represent **deployment-grade** (rather than purely theoretical) hydrogen production potential.

5.1. From PV DC atlas to electrical power available for electrolysis

Let $P_{DC,\beta}(t)$denote the PV DC power time series obtained at each grid cell for tilt β on the 1 km^2 parcel. The electrical power delivered to the electrolysis interface is obtained by applying an aggregate power conditioning efficiency η_{pc}, which accounts for conversion and balance of plant electrical losses between the PV DC bus and the electrolysis input [57].

$$P_{EL,\beta}(t) = \eta_{pc}P_{DC,\beta}(t) \tag{18}$$

Where η_{pc} is an aggregate power conditioning efficiency (e,g., DC/DC conversion,wiring and auxiliary losses).

The corresponding annual electrical energy supplied to electrolysis is computed by temporal integration

$$E_{EL,\beta} = \sum_t P_{EL,\beta}(t)\ \Delta t \tag{19}$$

When a rated interface limit is required (e.g., to avoid unrealistic utilization of short PV peaks or to represent constrained conversion capacity), the delivered electrolysis power is bounded by a rated value P_{EL}^{rated}

$$P_{EL,\beta}(t) min\left(\eta_{pc}P_{DC,\beta}(t), P_{EL}^{rated}\right) \tag{20}$$

where P_{EL}^{rated} is the Electrolyzer rated (nameplate) electrical input power (maximum admissible power at the Electrolyzer interface). In this study, P_{EL}^{rated} is set to the selected Electrolyzer capacity for the considered scenario, and Eq. (21) clips $\eta_{pc}P_{DC,\beta}(t)$to this rated limit to avoid overestimation from short PV power peaks.

The outputs of this step are $P_{EL,\beta}(t)$ and $E_{EL,\beta}$for both β = 0° and β = β*. These quantities form the energetic basis for hydrogen conversion and, later, the cost modelling.

[3] https://github.com/sandialabs/MATLAB_PV_LIB/blob/master/Example%20Data/SandiaModuleDatabase_20120925.xlsx?utm_source=chatgpt.com

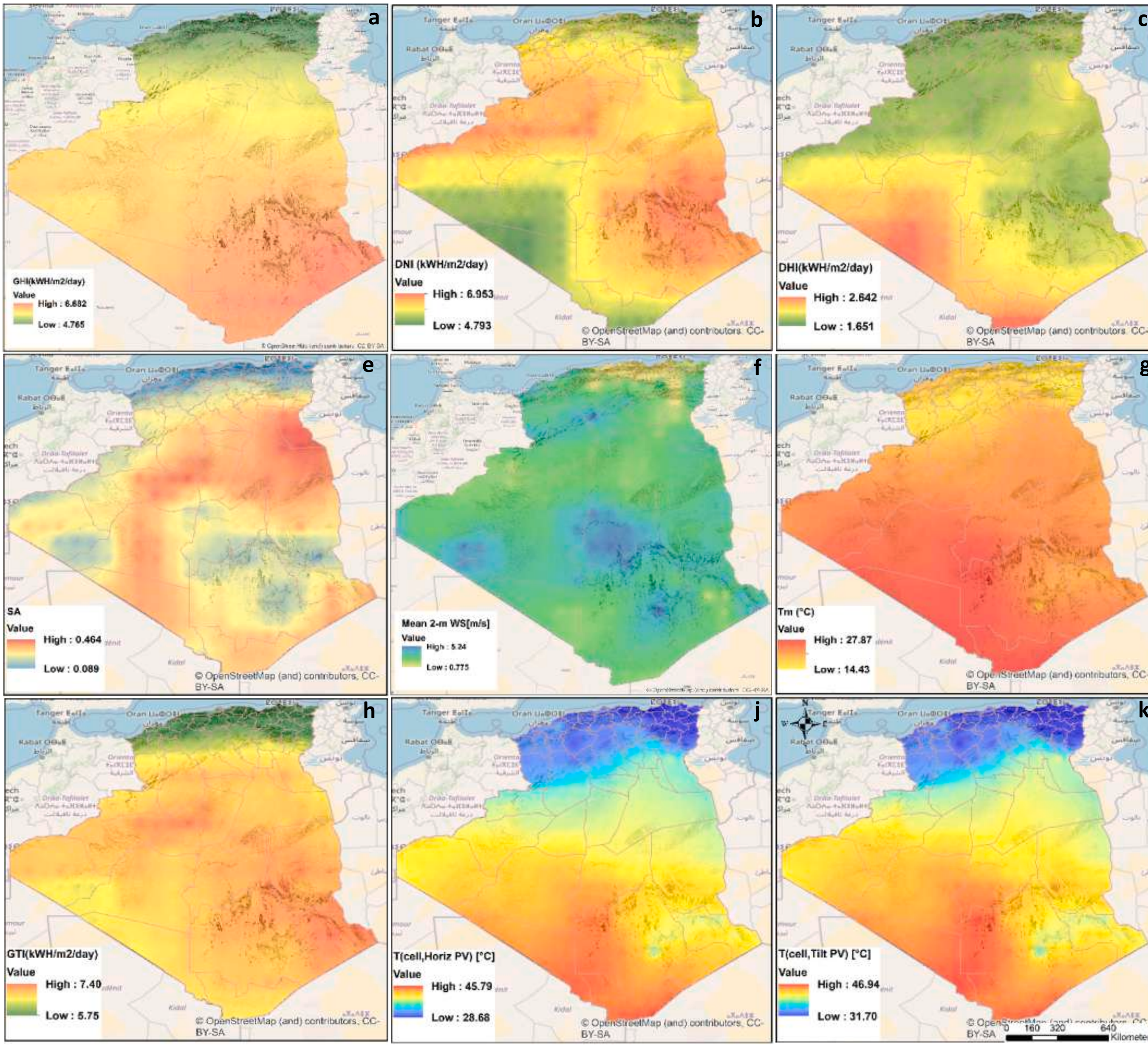

Fig. 4. Spatial distribution of PV resource and performance drivers across Algeria (inputs to the PV atlas) (a) global horizontal irradiation (GHI), **(b)** direct normal irradiation (DNI), **(c)** diffuse horizontal irradiation (DHI), **(e)** surface albedo, **(f)** wind speed, **(g)** ambient air temperature, **(h)** calculated global tilted irradiation (GTI, optimum tilt), **(j)** estimated PV cell temperature (horizontal configuration), **(k)** estimated PV cell temperature (optimally tilted configuration),

5.2. Conversion from electrical energy to hydrogen production (HHV basis)

Hydrogen production is computed using an HHV based electrolysis efficiency. The electrolysis performance is defined as the ratio of the chemical energy stored in the produced hydrogen (HHV) to the electrical energy supplied to electrolysis, the Electrolyzer's efficiency η_{EZ} is estimated from [58].

$$\eta_{EZ} = \frac{HHV_{H2} m_{H2}}{E_{EL,\beta}} \tag{21}$$

were $E_{EL}(kWh)$ is the electrical energy delivered to the electrolysis, $HHV_{H2} = 39.39 kWh/kg$ is the higher heating value of hydrogen, and $m_{H2,\beta}$ is the produced hydrogen mass. Rearranging gives the atlas conversion used at each grid cell

$$m_{H2,\beta} = \frac{\eta_{EZ}}{HHV_{H2}} E_{EL,\beta} \tag{22}$$

6. Techno-economic assessment and environmental performance metrics

To evaluate deployment grade PV–H_2 options across Algeria, we quantify both (i) the unit hydrogen production cost and (ii) screening level environmental benefits. The economic analysis computes the levelized cost of hydrogen (LCOH, €/kg) using a discounted cash flow formulation that accounts for PV and Electrolyzer capital expenditures. In parallel, environmental indicators are reported in terms of avoided CO_2 emissions and indicative natural gas displacement relative to conventional grey hydrogen benchmarks.

6.1. PV Electrolyzer system sizing and operating profile

A utility scale Electrolyzer of rated power $P_{EZ} = 50\ \boldsymbol{MW}$ is considered as the reference plant. To reflect an operational strategy where the Electrolyzer is not run continuously, its annual operating hours are defined as $H_{EZ} = n \times 365\ (h/year)$,with $n = 7.5\ h/day$.The corresponding target annual electricity demand at the Electrolyzer input is $P_{EZ}.H_{EZ}$.

For each grid cell, the required PV plant nameplate capacity is sized using the **local PV capacity factor**, and the assumed inverter efficiency. In other words, PV capacity is chosen such that the expected annual AC energy delivered by the PV plant (capacity factor × installed capacity × 8760 h, adjusted by an electrical conversion rate) meets the Electrolyzer's annual electricity requirement. This yields a **location dependent PV size** higher capacity factor regions require less PV capacity for the same 50 MW Electrolyzer operating profile.

6.2. Levelized cost of hydrogen (€/kg)

LCOH is computed as the ratio of discounted lifetime costs to discounted lifetime hydrogen production [57,58].

$$LCOH = \frac{C_0 + \sum_{y=1}^{N} \frac{C_y}{(1+r)^y}}{\sum_{y=1}^{N} \frac{M_y}{(1+r)^y}} \tag{23}$$

were

- N is the project lifetime (years)
- r is the real discount rate (%)
- C_0 is the initial investment (€)
- C_y is the cost occurring in year y (€/year)
- M_y is the hydrogen produced in year y (kg/year)

Initial investment $\boldsymbol{C_0}$. The upfront cost include PV CAPEX and Electrolyzer CAPEX, with a balance of plant/overhead adder

$$C_{PV} = PV_{capacity} \times PV_{CAPAX}$$

$$C_{EZ} = P_{EZ} \times Electrolyser_{CAPAX}$$

- $C_0 = (C_{PV} + C_{EZ})(1 + \varnothing)$,where $\varnothing$ is the overhead factor.

Annual cost $\boldsymbol{C_y}$. In this study, C_y includes

- **Fixed O&M** applied as fraction of PV and Electrolyzer CAPEX (EXCLUDING OVERHEAD)

$$C_{O\&M} = f_{PV} C_{pv} + f_{EZ} C_{EZ} \tag{24}$$

f_{PV} and f_{EZ} represent the annual fixed O&M rates (as a fraction of CAPEX per year) for the PV plant and Electrolyzer, respectively.

- **Stack replacement** as a discrete event in a specified replacement year $y = y_{rep}$

$$C_{rep}(y) = \begin{cases} \gamma C_{EZ}(1+\varphi), y = y_{rep} \\ 0, otherwise \end{cases} \tag{25}$$

The Electrolyzer stack is replaced **twice** over the project lifetime (at $y_{rep,1}$, and $y_{rep,2}$); γ is the stack replacement fraction, CEZ the initial Electrolyzer CAPEX, and φ the overhead/balance-of-plant adder.

Thus

$$C_y = C_{O\&M} + C_{rep}(y) \tag{26}$$

6.3. Environmental indicators avoided CO_2 emissions and natural gas displacement

To complement the techno economic results, two screening level environmental indicators are derived at each grid cell from the **land normalized hydrogen production atlas** (i) **avoided CO_2 emissions** and (ii) **displaced natural gas (NG) consumption**, both referenced to a conventional **grey hydrogen** baseline. Because the hydrogen atlas is already expressed per standardized **1 km^2 parcel** and accounts for the **effective PV occupation fraction** adopted in this study, the indicators below represent *deployment grade.*

(a) **Avoided CO_2 emissions relative to grey hydrogen**

Let $M_{H2}(x)$ denote the annual hydrogen production at grid cell, expressed per unit surface area (tonnes of H_2 per km2 per year)

$$M_{H2}(x)[t.H_2.sq.km/yr] \tag{27}$$

Assuming PV powered electrolysis has negligible direct operational emissions at the point of production, the avoided CO_2 emissions are computed by multiplying the hydrogen yield by a plant gate emission factor [59].

$$CO_{2,avoided}(x) = EF_{grey}\ M_{H2}(x) \tag{28}$$

were $EF_{grey} = 12\ kg.CO_2/kg.H_2$, is the grey-hydrogen emission factor, expressed as the **mass of CO_2 per mass of H_2.** The resulting map is reported as

$$CO_{2,avoided}(x)\ [t.CO_2.sq.km/yr] \tag{29}$$

(b) Natural gas displacement associated with grey hydrogen replacement.

In the same manner, the avoided natural gas consumption is estimated using an SMR equivalent gas requirement per unit hydrogen [60].

$$NG_{saved}(x) = k_{NG} M_{H2}(x) \tag{30}$$

$$NG_{saved}^{Nm^3} = k_{NG}^{Nm^3}\ MH_2(x), k_{NG}^{Nm^3} = 4730Nm^3 \Big/ t.H_2 \tag{31}$$

7. Results and interpretation

This section reports the spatial outputs of the proposed PV-to-hydrogen screening framework for Algeria under four deployment cases: (i) unconstrained technical potential, (ii) grid-connected eligibility, (iii) North–South (N—S) corridor-enabled feasibility, and (iv) remote/off-grid feasibility, each evaluated for two PV configurations (horizontal and optimal tilt). Results are presented in the order of the modelling chain: (1) land-normalized PV DC electricity yield (GWh/km^2·yr), (2) green hydrogen production density, (3) spatial LCOH, and (4) screening-level environmental indicators (CO_2 avoidance and indicative natural gas displacement relative to a grey hydrogen baseline).

To distinguish resource abundance from deployment feasibility, it is important to note that the scenario masks do not modify the solar resource; they restrict the land domain to represent alternative planning logics and infrastructure conditions. Therefore, differences between scenarios quantify shifts from technical potential to deployable potential, highlighting how grid access, corridor development, and remote deployment assumptions reshape the portfolio of high-yield and low-cost zones.

7.1. PV DC yield atlas under four deployment scenarios (horizontal vs optimal tilt)

The primary spatial driver of all downstream maps (H_2 density, LCOH, and avoided emissions) is the annual PV DC yield per unit land area (GWh/km^2·yr), as shown in Figs. 5–6.

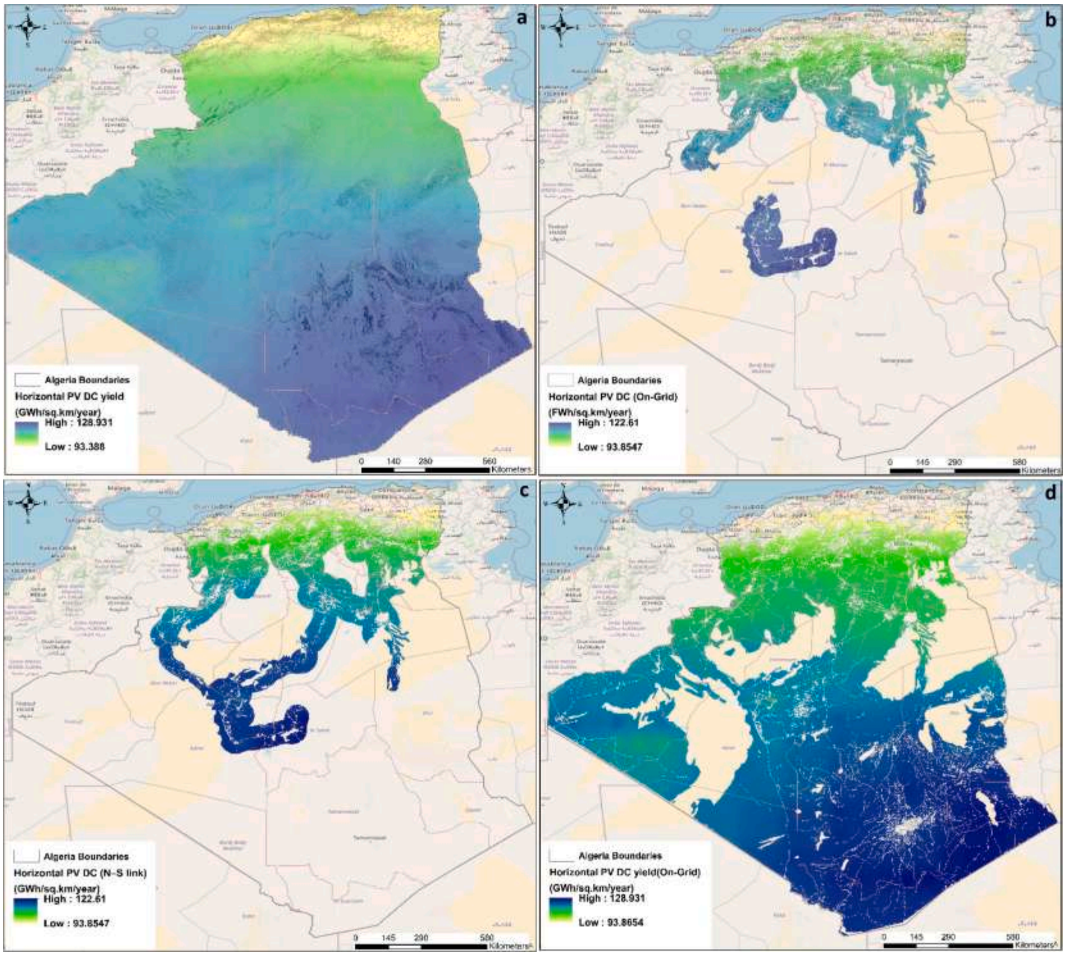

Fig. 5. Spatial distribution of horizontal PV DC yield in Algeria, ***(a)*** Baseline horizontal PV DC yield across Algeria (GWh/km^2/year), ***(b)*** Horizontal PV DC yield for on-grid eligible areas (GWh/km^2/year), ***(c)*** Horizontal PV DC yield for the on-grid N—S link corridor (GWh/km^2/year), ***(d)*** Horizontal PV DC yield (Off-grid) across Algeria (GWh/km^2/year).

1. **Magnitude and spatial contrast (unconstrained case).**

The unconstrained (technical potential) PV–DC yield spans **~93–129 GWh/km^2·yr** for **horizontal** and **~ 111–142 GWh/km^2·yr** for **tilted** systems, confirming strong geographic variability and a clear advantage for optimized tilt. This resource contrast will later appear almost linearly in the hydrogen production density maps (because H_2 output is proportional to delivered DC energy through fixed conversion efficiencies).

2. **Effect of scenario feasibility masks (resource capture vs resource existence).**

Moving from unconstrained to **grid connected eligibility** reduces the developable domain and slightly lowers the observed upper tail (e.g., horizontal max drops from ~129 to ~123 GWh/km^2·yr), indicating that **some top yield land is not immediately collocated with current grid accessible areas**. The **N—S corridor scenario** expands feasible land into the interior and recovers access to additional high yield zones showing that corridor planning primarily improves **the ability to capture high resource,** not the resource itself. The **off grid remote scenario** retains (or recovers) near maximum yields because it includes remote interior areas with strong solar potential, but it implies a different development model where **infrastructure and logistics not energy yield become the binding constraints** (water supply, transport/export chain, and site access).

3. **Horizontal vs tilt why this matters economically.**

Allowing tilt yields an uplift of roughly **~10–20%** (countrywide order of magnitude), and it tends to make more of the grid eligible footprint **competitively productive**. This is important for the cost and policy narrative higher DC yield improves Electrolyzer utilization per unit PV land and reduces the electricity driven component of **LCOH**, particularly in areas where development is constrained to the existing grid footprint.

7.2. Hydrogen production atlas under four deployment scenarios (horizontal vs optimal tilt)

The hydrogen production maps translate the PV–DC resource into **land normalized green hydrogen output** using the fixed conversion chain defined in the methods (DC coupled PV → DC/DC → Electrolyzer). As a result, the mapped indicator **hydrogen production density** ***($t{\cdot}km^{-2}{\cdot}yr^{-1}$)*** inherits the spatial structure of PV–DC yield, while the four scenarios primarily control **where** this potential can be realized under differing infrastructure and accessibility assumptions (Figs.7–8).

(1) Unconstrained technical potential spatial signal and magnitude.

Under the unconstrained case (panel *a* in each figure), hydrogen production density shows a clear spatial gradient across Algeria. For horizontal PV, the mapped range is ~1831–2528 t·km^{-2}·yr^{-1}, whereas for tilted PV it increases to ~2184–2775 t·km^{-2}·yr^{-1}. These values provide a direct, land based measure of "how much H_2 a km^2 can

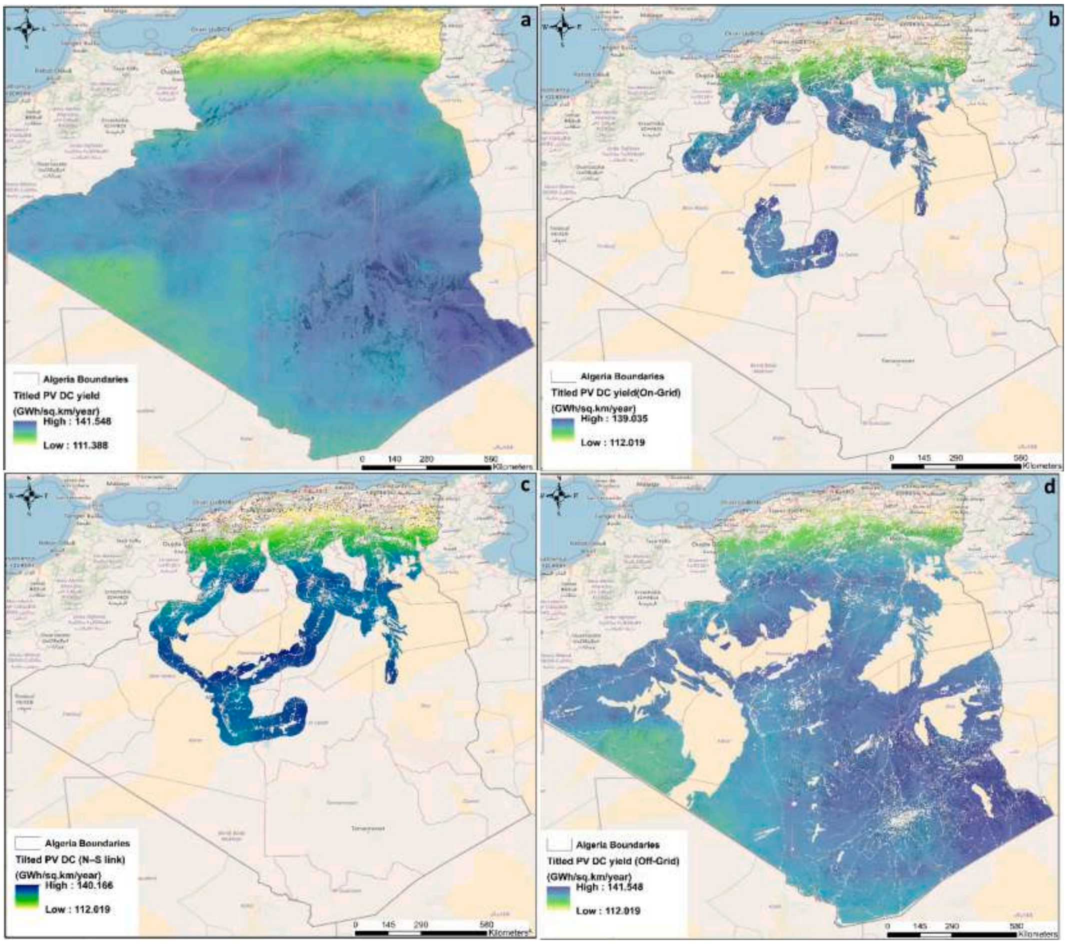

Fig. 6. Spatial distribution of Titled PV DC yield in Algeria, ***(a)*** Baseline Titled PV DC yield across Algeria (GWh/km^2/year), ***(b)*** Titled PV DC yield for on-grid eligible areas (GWh/km^2/year), ***(c)*** Titled PV DC yield for the on-grid N—S link corridor (GWh/km^2/year), ***(d)*** Titled PV DC yield (off-grid) across Algeria (GWh/km^2/year).

produce," given the assumed PV packing and conversion efficiencies, and they establish the upper envelope that later cost and impact maps will build upon.

(2) Effect of scenario masks feasibility reshapes the map more than it changes the range.

Moving from the unconstrained case to the grid connected eligibility scenario (panel *b*) primarily removes large portions of high potential territory from consideration, concentrating feasible production into the current grid accessible footprint. This filtering slightly reduces the upper tail (e.g., horizontal max ~2404 t·km^{-2}·yr^{-1} and tilted max ~2726 t·km^{-2}·yr^{-1}) while leaving the lower bound close to the unconstrained minimum. In planning terms, the key message is not that the resource disappears, but that bankable deployment opportunities depend strongly on infrastructure alignment.

(3) N—S corridor scenario "resource capture" improves relative to grid only.

The North–South interconnection corridor (panel *c*) expands feasible production beyond the current grid accessible envelope and reconnects portions of the interior where PV driven hydrogen productivity is competitive. This is reflected by corridor maxima that approach (or partially recover toward) the unconstrained upper tail (e.g., tilted max ~2748 t·km^{-2}·yr^{-1}). The corridor therefore functions as an enabling strategy it increases the share of high yield land that can realistically contribute to hydrogen supply without requiring fully remote, standalone project architectures.

(4) Off grid remote scenario high productivity remains available, but the constraint shifts from energy to logistics.

In the off grid eligible scenario (panel *d*), the accessible domain moves toward remote land (by construction, away from roads/grid/settlements), while the achievable production densities remain close to the unconstrained case (e.g., horizontal max ~2528 t·km^{-2}·yr^{-1}; tilted max ~2775 t·km^{-2}·yr^{-1}). This highlights a crucial development insight high output hydrogen hubs are feasible in remote regions, but the dominant constraints become water supply, site logistics, and hydrogen transport/export infrastructure, rather than the solar resource itself.

(5) Horizontal vs tilted PV systematic uplift with scenario stable ranking.

Across all scenarios, tilt consistently increases hydrogen production density, with an uplift on the order of ~10–20% relative to horizontal mounting (depending on location). Importantly, tilt tends to preserve the relative ranking of high vs low productivity zones while improving absolute output, which later translates into more favorable economics (higher effective utilization of PV land and lower cost per unit H_2 for a given investment envelope). Because hydrogen production density scales directly with delivered PV–DC energy, these spatial patterns propagate into the subsequent LCOH and CO_2/NG displacement maps, while scenario differences continue to reflect feasibility and infrastructure rather than changes in the underlying resource.

7.3. Spatial levelized cost of hydrogen under PV driven electrolysis CAPEX context and scenario results (horizontal vs tilted PV)

Before interpreting the LCOH maps, it is important to position the **investment cost assumptions** relative to the wider literature. A large

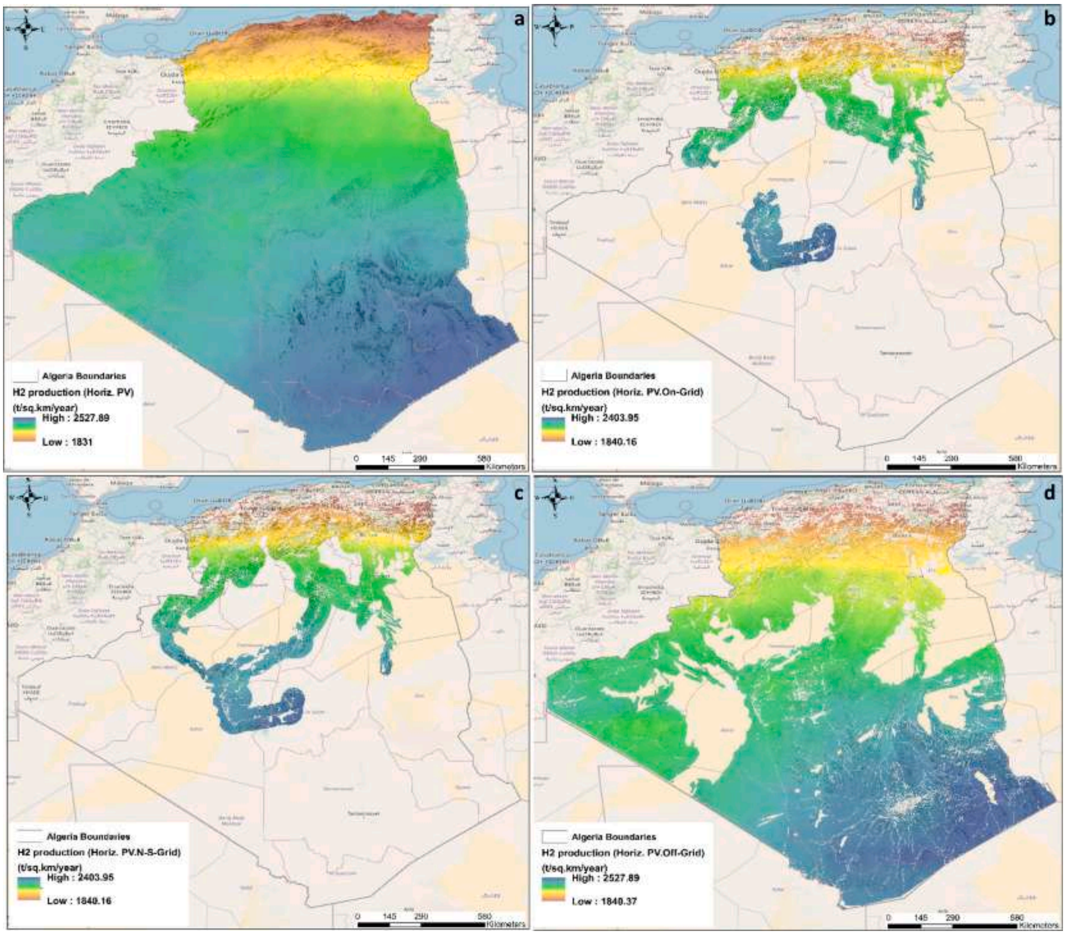

Fig. 7. Spatial distribution of hydrogen production potential from horizontal PV across Algeria under grid-availability scenarios (a) baseline (unconstrained) hydrogen production density, **(b)** hydrogen production in on-grid eligible areas, **(c)** hydrogen production along the on-grid North–South (N—S) interconnection corridor, and **(d)** hydrogen production in the off-grid eligible scenario. **Units** *($t \cdot km^{-2} \cdot yr^{-1}$)*.

share of published spatial studies adopts **optimistic/low CAPEX inputs,** commonly reporting utility scale PV costs in the **~300–754 USD/kW** range and Electrolyzer costs around **~500–788 USD/kW** [61–64]. In practice, reported costs are **highly context dependent** (region, supply chain, scope of "installed cost", and balance of plant). For PV, global benchmarks indicate a 2023 weighted average installed cost of about **758 USD/kW** for utility scale systems, while country specific ranges can be wider [65]. For Electrolyzer, recent evidence highlights even stronger divergence **installed** system costs outside China in 2024 are reported in the **~2000–2600 USD/kW** range, whereas Chinese manufactured and installed systems are commonly lower (e.g., **~600–1200 USD/kW**), depending on technology and scope [66].

In the present study, the PV and Electrolyzer CAPEX values are taken from a **recent Fraunhofer ISE (2024) cost basis** (Appendix A) to represent a **near term, conservative** investment case suitable for publication grade screening [67]. This choice reduces the risk of systematically underestimating LCOH that can arise when using "best case" CAPEX assumptions that may not reflect full installed system costs or regional procurement conditions.

Across all scenarios, the spatial LCOH patterns closely follow the annual hydrogen production maps, as shown in Figs. 9–10 regions with higher annual hydrogen output density exhibit lower LCOH, because fixed capital expenditures are amortized over more kilograms of hydrogen. The scenario masks (grid only, N—S corridor, off grid) do not change the underlying solar resource or conversion chain; they mainly determine which parts of the country can realize low cost production under each infrastructure logic.

- For **tilted PV**, LCOH spans approximately **4.64–5.24 €/kg H_2** (baseline/unconstrained), with very similar ranges under the filtered scenarios (e.g., on grid ~**4.68–5.22 €/kg**, corridor ~**4.67–5.22 €/kg**, off grid ~**4.64–5.22 €/kg**).
- For **horizontal PV**, LCOH is systematically higher, spanning approximately **4.86–5.77 €/kg H_2** (baseline), with on grid and corridor cases around **~4.98–5.76 €/kg**, and off grid again approaching the baseline lower bound (**~4.86 €/kg**).

This implies a tilt driven cost reduction of roughly **0.2–0.6 €/kg H_2** across the mapped domain (largest reductions appearing where Hydrogen productivity gains are most valuable), confirming that optimal tilt is not only an energy yield improvement but also a **system level economic lever.**

A decomposition of the minimum cost case (LCOH = **4.64 €/kg H_2**) confirms that the costs are dominated by upfront investments (Fig. 11 and Table 2). **PV CAPEX (39.8%, 1.84 €/kg H_2)** and **Electrolyzer CAPEX (37.4%, 1.73 €/kg H_2)** together account for ~**77%** of total LCOH, while **stack replacement** contributes **8.4%** (0.39 €/kg H_2). Fixed O&M remains secondary, with **PV OPEX (7.3%, 0.34 €/kg H_2)** and **Electrolyzer OPEX (7.2%, 0.34 €/kg H_2)** contributing comparable shares. This structure explains why the spatial patterns are highly sensitive to hydrogen productivity (which amortizes CAPEX through higher annual hydrogen output) and why projected CAPEX reductions translate directly into large downward shifts in LCOH.

To assess the robustness of the minimum-cost estimate and quantify the influence of key assumptions, Fig. 12 presents a targeted sensitivity

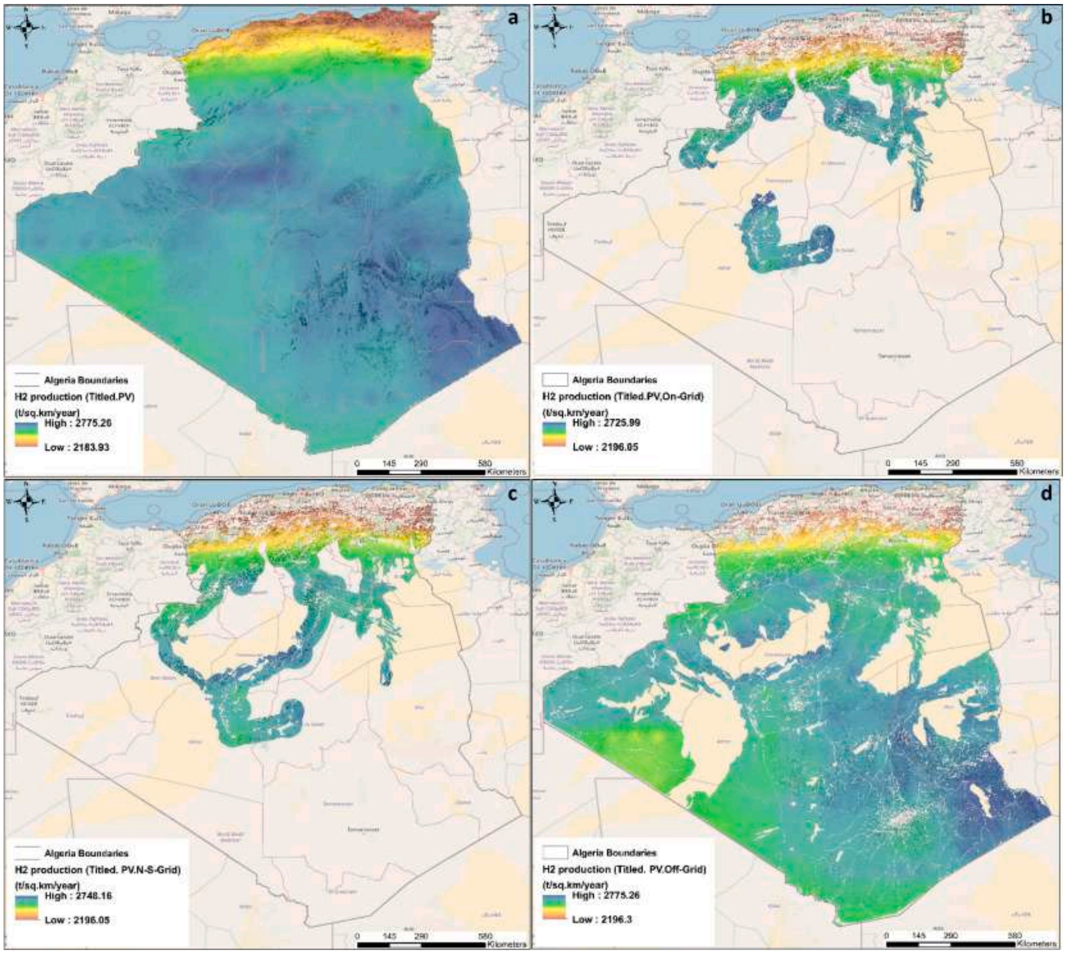

Fig. 8. Spatial distribution of hydrogen production potential from Titled PV across Algeria under grid-availability scenarios (a) baseline (unconstrained) hydrogen production density, **(b)** hydrogen production in on-grid eligible areas, **(c)** hydrogen production along the on-grid North–South (N—S) interconnection corridor, and **(d)** hydrogen production in the off-grid eligible scenario. **Units** *($t{\cdot}km^{-2}{\cdot}yr^{-1}$)*.

analysis at the best-performing location. Two-parameter sweeps were performed for the dominant drivers identified in the cost breakdown: PV CAPEX, Electrolyzer CAPEX, discount rate, and Electrolyzer efficiency. The sensitivity surfaces show a strong, monotonic increase in LCOH with both PV and Electrolyzer CAPEX, consistent with their dominant contribution in Fig. 11/Table 2. Financing conditions introduce an additional systematic effect: higher discount rates increase LCOH across the full CAPEX space, reflecting the capital-intensive nature of PV–Electrolyzer systems. Improvements in Electrolyzer efficiency reduce LCOH through increased hydrogen yield per unit of delivered electricity; however, within realistic efficiency bounds, the magnitude of this effect is generally smaller than comparable relative changes in CAPEX or discount rate. Across the explored parameter space in Fig. 12, best-site LCOH spans approximately 2.269–7.62 €/kg H_2, highlighting that absolute cost levels are strongly dependent on technology cost trajectories and financing assumptions, even when resource conditions are fixed.

Building on the resource-driven improvements achieved through optimal tilt, the scenario filtering indicates that infrastructure feasibility primarily governs the realizable geography of low-cost hydrogen. In the unconstrained technical potential, minimum LCOH values align with the highest PV-to-H_2 productivity, defining the cost frontier implied by the assumed techno-economic parameters. When deployment is restricted to grid-eligible land, the feasible portfolio contracts to the existing network footprint, excluding portions of low-cost interior territory. The proposed North–South corridor partially alleviates this constraint by extending grid reach into higher-productivity zones, thereby increasing the accessible share of low-LCOH land relative to a grid-only strategy. Conversely, the off-grid eligibility mask recovers much of the low-cost envelope, indicating that competitive production is achievable in remote regions; however, in this configuration the binding constraints shift from solar resource quality to project enablers such as water provision and hydrogen logistics/transport. Overall, the maps indicate that while tilt optimization improves competitiveness consistently, infrastructure and deployment assumptions primarily determine the scale and spatial availability of cost-competitive hydrogen, more than they alter the resource-based ranking of sites.

7.4. Environmental co benefits of PV based green hydrogen avoided CO_2 emissions and natural gas savings

The avoided-CO_2 and natural-gas displacement maps reported in this section are **screening indicators** computed from the hydrogen production atlas using the grey-hydrogen reference factors defined in Section 6.3. They quantify the **operational substitution benefit at the point of production** and do not represent a full ISO-compliant life-cycle assessment (LCA) of PV-electrolysis hydrogen. Upstream and downstream life-cycle contributions including PV/Electrolyzer manufacturing and replacements, balance-of-plant and civil works, water treatment where relevant, and hydrogen conditioning (compression/storage) and transport/export logistics are not explicitly modeled; results should therefore be interpreted as **mitigation-potential intensity** rather than a cradle-to-gate product footprint [68].

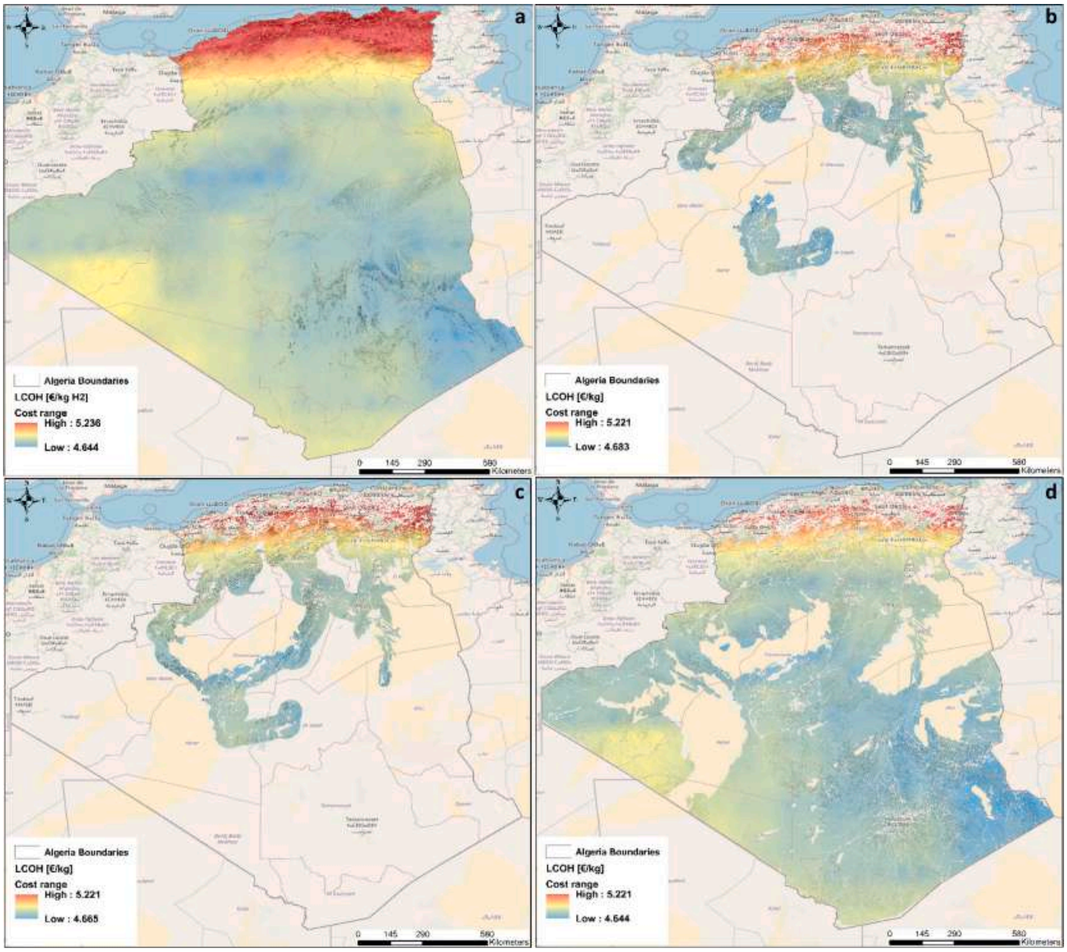

Fig. 9. Spatial distribution of the levelized cost of hydrogen (LCOH) from tilted PV-driven electrolysis across Algeria under grid-availability scenarios (a) baseline (unconstrained) LCOH, (b) LCOH in on-grid eligible areas, (c) LCOH along the on-grid North–South (N—S) interconnection corridor, and (d) LCOH in the off-grid eligible scenario. Units (€/kg H_2).

7.4.1. Avoided CO_2 emissions (kt $CO_2 \cdot km^{-2} \cdot yr^{-1}$)

The avoided CO_2 maps indicate a strong and spatially coherent mitigation potential per unit land area, with **tilted PV** delivering systematically higher avoidance than **horizontal PV**, consistent with its higher hydrogen productivity (Figs.13–14). In the unconstrained baseline, avoided emissions span approximately **26.21–33.30 kt $CO_2 \cdot km^{-2} \cdot yr^{-1}$** for tilted PV, compared with **21.97–30.33 kt $CO_2 \cdot km^{-2} \cdot yr^{-1}$** for horizontal PV. Across the grid eligibility and corridor scenarios, the feasible domain contracts to infrastructure compatible land and the upper tail is modestly reduced (e.g., tilted maxima around **~32.7–33.0,** horizontal maxima around **~28.8),** reflecting the fact that the highest productivity interior zones are not fully captured by the present grid footprint. The proposed N—S corridor partially restores access to higher productivity areas and therefore recovers a larger share of high avoidance locations relative to a strict grid only case. In the off grid scenario, the attainable avoidance per unit area returns close to the unconstrained envelope, indicating that remote regions retain very high mitigation intensity, albeit with feasibility dominated by non-resource constraints (notably water provision and hydrogen logistics).

7.4.2. Natural gas savings ($MNm^3 \cdot km^{-2} \cdot yr^{-1}$)

The natural gas displacement maps exhibit the same spatial logic as avoided CO_2, as both metrics are proportional to green hydrogen output and reference the same grey hydrogen counterfactual. Under the unconstrained baseline, **tilted PV** yields roughly **10.33–13.13 $MNm^3 \cdot km^{-2} \cdot yr^{-1}$** of gas savings, while **horizontal PV** yields about **8.66–11.96 $MNm^3 \cdot km^{-2} \cdot yr^{-1}$ (**Figs.15–16). Grid eligible filtering again narrows the feasible geography and slightly reduces the maximum savings (tilted maxima around **~12.9**, horizontal around **~11.4),** whereas the N—S corridor increases the reachable share of high savings land by extending feasibility into more productive zones. The off grid scenario recovers near maximum savings intensities (tilted up to **~13.18,** horizontal up to **~11.95),** reinforcing that Algeria's remote high resource areas can deliver strong climate and fuel saving co benefits per unit land, provided enabling infrastructure (water and transport/export) is addressed.

8. Discussion export oriented production scenarios and Algeria–Europe outlook

The atlas results show that Algeria's PV-to-hydrogen competitiveness is governed by the interaction of (i) **resource productivity,** which defines the cost frontier, and (ii) **enabling infrastructure,** which determines how much of that frontier is practically reachable. This tradeoff is visible across the scenario filters: grid eligibility concentrates feasible deployment into the existing footprint, the proposed N—S corridor improves access to interior high-productivity zones, and the off-grid case recovers much of the technical envelope while shifting constraints from resource quality toward **water provision and hydrogen logistics/transport.**

The cost structure at the minimum-LCOH site confirms that outcomes are predominantly **CAPEX-driven**, so higher PV-to-H_2 productivity reduces unit cost mainly by amortizing PV and Electrolyzer

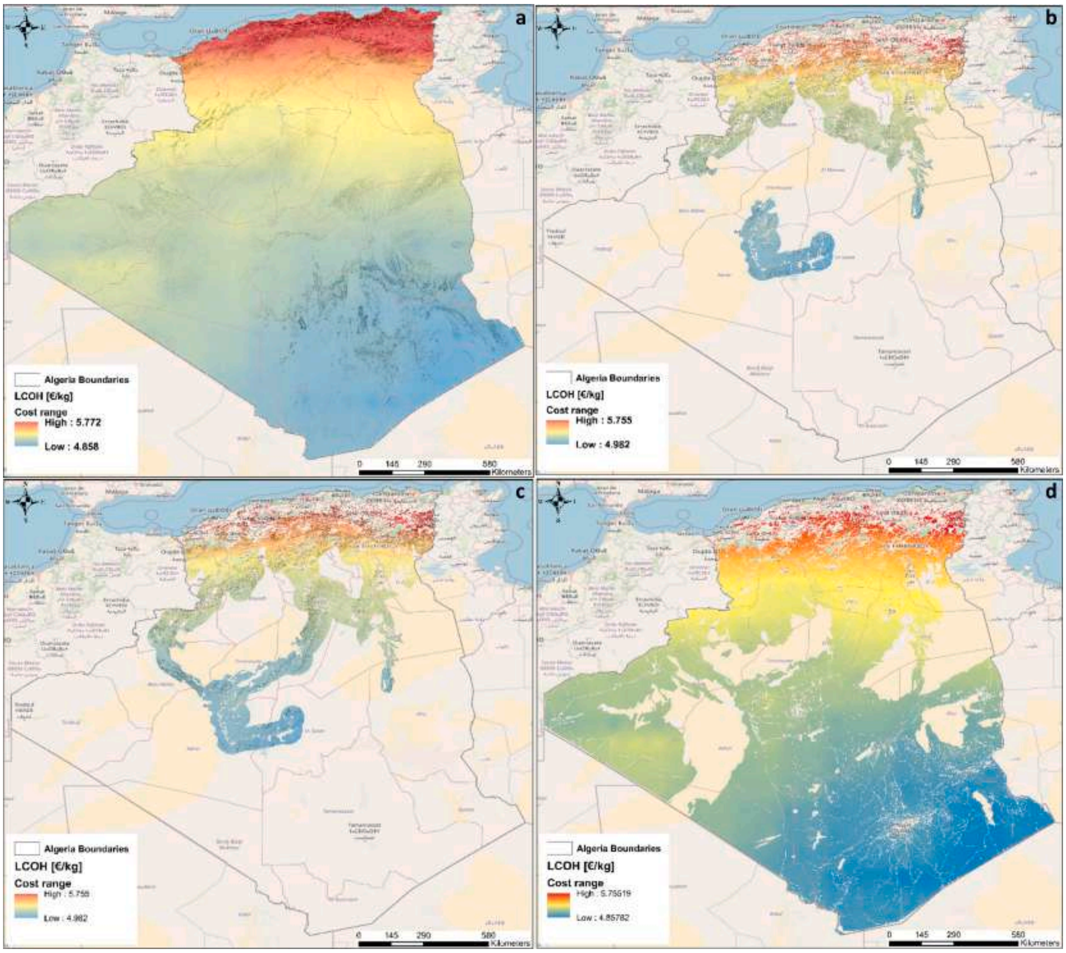

Fig. 10. Spatial distribution of the levelized cost of hydrogen (LCOH) from Horizontal PV-driven electrolysis across Algeria under grid-availability scenarios (a) baseline (unconstrained) LCOH, (b) LCOH in on-grid eligible areas, (c) LCOH along the on-grid North–South (N—S) interconnection corridor, and (d) LCOH in the off-grid eligible scenario. Units (€/kg H_2).

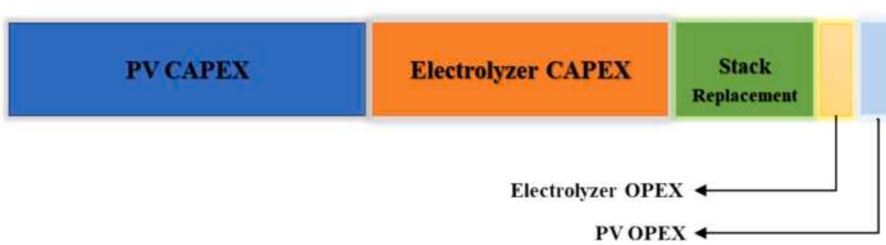

Fig. 11. LCOH cost structure for the lowest cost case (LCOH = 4.64 €/kg H_2).

Table 2
LCOH decomposition for the lowest cost location (4.64 €/kg H_2).

Component	Share	€/kg H_2
PV CAPEX	39.8%	1.84
Electrolyzer CAPEX	37.4%	1.73
Stack Replacement	8.4%	0.39
PV OPEX	7.3%	0.34
Electrolyzer OPEX	7.2%	0.34

investments over larger annual hydrogen output. This framing supports a phased planning logic: near-term hubs can prioritize locations with adequate productivity and low implementation friction (grid/industrial interfaces), while medium-term scale-up depends on targeted corridor investments and integrated water–logistics planning to unlock interior high-productivity regions.

For export-oriented interpretation, infrastructure reports indicate that large-volume hydrogen delivery is consistent with corridor concepts, and that long-distance pipeline transport can be cost-competitive once built (order-of-magnitude levelized transport costs **€0.11–0.21/kg per 1000 km** for onshore segments; higher for fully offshore routing) [69]. At the same time, recent Europe–North Africa co-optimization modelling highlights that large export volumes require rapid renewable-system expansion and can shift substantial build-out burdens to exporting regions, reinforcing that atlas-based export scenarios should be read as **screening pathways** that motivate follow-on corridor-level design and scheduling analysis [70].

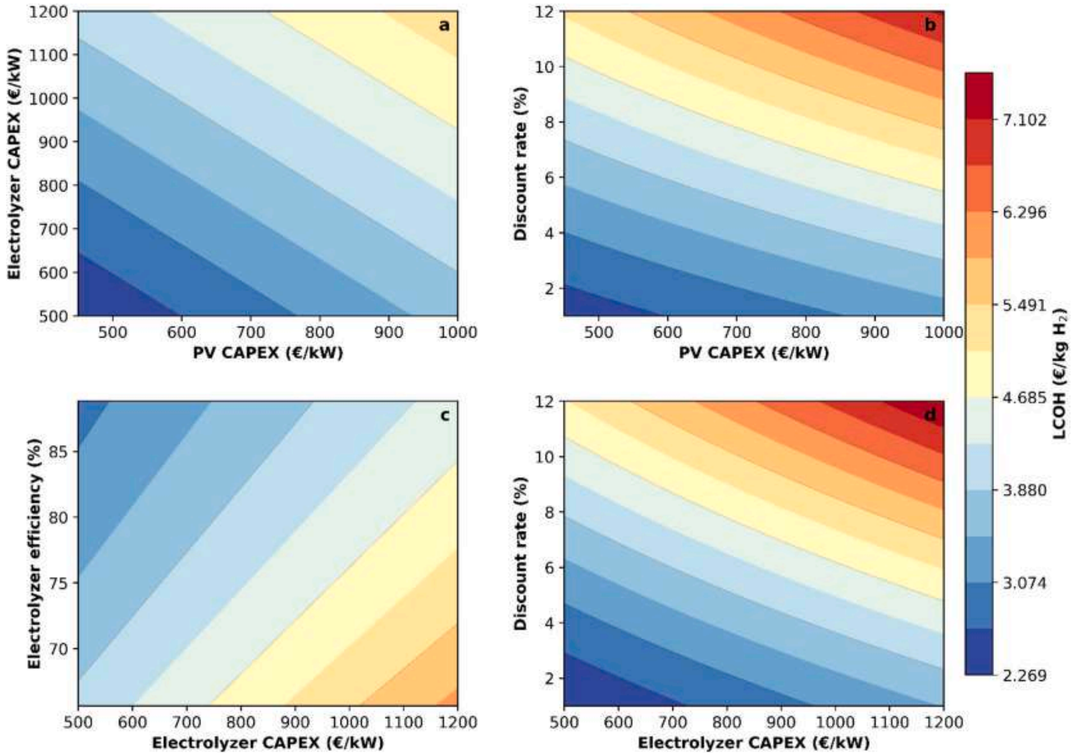

Fig. 12. LCOH sensitivity (€/kg H_2): (a) PV CAPEX vs. Electrolyzer CAPEX; (b) PV CAPEX vs. discount rate; (c) Electrolyzer CAPEX vs. Electrolyzer efficiency; (d) Electrolyzer CAPEX vs. discount rate.

8.1. Scenario 1 supplying 10 Mt. $H_2 \cdot yr^{-1}$ from inland hubs land requirement, water feasibility, and pipeline export routing

Scenario 1 evaluates two representative inland production hubs Ain Salah (higher solar/H_2 productivity) and Laghouat (lower productivity but closer to northern infrastructure and coastal export interfaces) to assess the feasibility of delivering an export scale tranche of 10 Mt. $H_2 \cdot yr^{-1}$ and linking it to (existing/proposed) Mediterranean export corridors.

Based on the hydrogen atlas, the **mean land normalized hydrogen production density** in the highlighted hub areas is **~2692 t·km^{-2}·yr^{-1}** for **Ain Salah (southern Algeria)** and **~ 2643 t·km^{-2}·yr^{-1}** for **Laghouat (north–central Algeria).** Converting these mean intensities into an export scale target of **10 Mt $H_2 \cdot yr^{-1}$** implies a required developable footprint of approximately **~3714 km^2** in Ain Salah and **~ 3784 km^2** in Laghouat.

Electrolysis has a fixed stoichiometric water requirement of ~9 L per kg H_2 (≈9 m^3 per tonne H_2) [70]. For 10 Mt. $H_2 \cdot yr^{-1}$, this corresponds to a minimum of ~90 million m^3·yr^{-1}. When including additional water associated with treatment/purification processes, total water demand can rise substantially; a synthesis estimate reports 9 L/kg (stoichiometric) plus 15 L/kg for treatment, (24 L/kg overall) which would imply 240 million m^3·yr^{-1} for 10 Mt. $H_2 \cdot yr^{-1}$ [71].

When benchmarked against the **Albian/NWSAS stored reserves** (Fig.17) often cited at **~60,000 billion m^3,** this represents only **~0.00015–0.00040% of the storage per year**, i.e., negligible relative to the *stock*. However, feasibility is better judged against **renewability** recharge for the NWSAS is widely reported to be on the order of **~1 billion m^3·yr^{-1},** meaning that producing 10 Mt. $H_2 \cdot yr^{-1}$ would require about **~9–24% of annual recharge** (depending on whether only stoichiometric water or a treatment inclusive value is adopted). Given that reported abstraction has already increased substantially (e.g., **~0.6 to ~ 2.5 billion m^3·yr^{-1}** over recent decades), this additional demand is **non-negligible** and should be treated as a potential constraint requiring **site-specific** hydrogeological and water-treatment assessment to determine whether the incremental withdrawals are acceptable without accelerating drawdown and salinization.

The Ain Salah option sits closer to peak PV/H_2 productivity, but its distance from the northern corridor and coastal export interfaces implies longer hydrogen transport (or conversion to a carrier) and a larger infrastructure burden. Laghouat, while somewhat lower in productivity, can become system preferable once the analysis shifts from *gate* metrics (H_2 per km^2) to *delivered* metrics, because it is better positioned for integration with the national pipeline network and Mediterranean export routes (Fig.18).

Scenario 1 therefore represents a city hub configuration, in which Electrolyzer s are assumed to be sited within the selected provinces and hydrogen is transported to demand or export interfaces via pipeline infrastructure. While the atlas based results provide a first order screening of production intensity, LCOH, and water requirements, further work is required to confirm technical and economic viability, including detailed routing and compression costs, right of way constraints, water sourcing and treatment design, and an integrated delivered cost assessment for the two suggested provinces.

8.2. Scenario 2 coastal desalination–integrated green hydrogen (treated seawater supply and renewable certified electricity)

Scenario 2 addresses the water availability constraint by anchoring export scale hydrogen production to **seawater desalination**, thereby avoiding sustained reliance on inland groundwater. In this configuration, Electrolyzer are conceptually **co located with (or directly supplied by) a coastal desalination plant,** and both the **electrolysis load and the desalination load** are assumed to be supplied by **clean electricity only** (i.e., dedicated PV supply and/or a renewable certified grid arrangement), so that the resulting hydrogen remains fully "green" without mixed grid emissions.

Using the stoichiometric electrolysis requirement of **9 L/kg H_2** (equivalently **9 m^3 per tons H_2)** as the design basis, producing **10 Mt $H_2 \cdot yr^{-1}$** requires approximately **90 million m^3·yr^{-1}** of treated water,

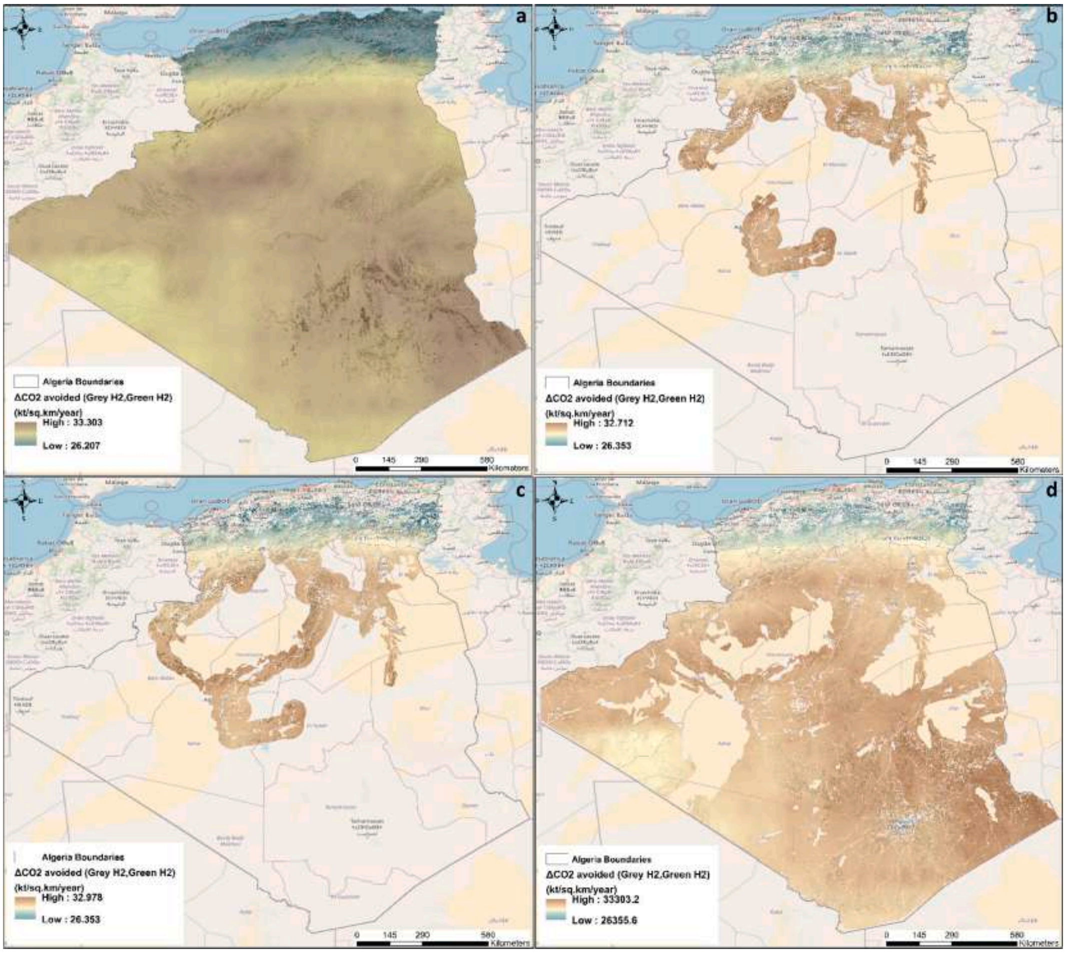

Fig. 13. Spatial distribution of avoided CO_2 emissions relative to grey hydrogen for tilted PV-driven hydrogen production across Algeria under grid-availability scenarios (a) baseline (unconstrained), (b) on-grid eligible areas, (c) on-grid North–South (N—S) interconnection corridor, and (d) off-grid eligible scenario. Units (kt CO_2·km^{-2}·yr^{-1}).

corresponding to an average flow of about **246,600 m^3/day.** Under the desalination portfolio listed in this study, the **Koudiet Eddraouche** seawater desalination plant (El Tarf) has a rated capacity of **300,000 m^3/day,** equivalent to **109.5 million m^3·yr^{-1}** of treated product water. On a purely volumetric basis, this capacity is sufficient to supply the stoichiometric feedwater needed for **10 Mt H_2·yr^{-1}.** Expressed as an equivalent hydrogen capacity, **300,000 m^3/day** of treated water could support up to **~12.2 Mt H_2·yr^{-1}** if fully allocated to electrolysis under the 9 L/kg assumption. In practice, final conditioning (polishing) to Electrolyzer grade water may still be required depending on the delivered water quality.

A central condition of Scenario 2 is electricity integrity. Even when desalinated water is available at the coast, the hydrogen cannot be considered fully green if either desalination or electrolysis is powered by a fossil mixed grid. Accordingly, Scenario 2 assumes a **clean grid boundary** desalination and electrolysis are supplied either by (i) a **dedicated PV plant** physically or contractually linked to the loads, or (ii) a **renewable certified supply** with clear traceability (e.g., contracted renewable generation matched to annual energy demand). This requirement is particularly relevant for export narratives, where certification frameworks increasingly scrutinize the electricity source and additionality.

Overall, Scenario 2 demonstrates (Fig. 19),that a **mega scale coastal desalination plant (300,000 m^3/day)** can, in principle, cover the **stoichiometric** water requirement associated with **10 Mt H_2·yr^{-1},** while shifting the feasibility discussion from groundwater sustainability to **coastal siting, desalination integration, and renewable power provisioning**. As with Scenario 1, this scenario remains a screening level configuration and requires further work on (i) the share of desalinated water realistically allocable to hydrogen, (ii) the required polishing train to Electrolyzer specifications, (iii) the dedicated renewable supply design and grid connection strategy, and (iv) an integrated delivered cost assessment including pipeline routing and compression.

8.3. Scenario 3 electricity export via mediterranean interconnection and end use electrolysis in Europe

Scenario 3 evaluates an alternative export logic in which Algeria's solar electricity is **exported as electricity** via grid reinforcement and a potential **Mediterranean HVDC interconnection** and **electrolysis is performed at the demand side.** This pathway is motivated by two structural considerations revealed by the atlas results (i) the highest PV driven hydrogen productivity in Algeria is often located in the interior, where **water supply and logistics** can become binding constraints, and (ii) hydrogen export by pipeline requires long, capital intensive corridor development. In contrast, exporting electricity shifts the conversion step (electrolysis) to the receiving system while allowing Algeria to monetize its solar resource through cross border power transfer.

From an infrastructure standpoint, the scenario can be framed as a two stage architecture on the Algerian side **(1) collection and northbound transmission**, using the national grid and/or a dedicated reinforcement corridor to bring renewable electricity from high yield regions toward coastal or northeastern nodes; and **(2) subsea HVDC export**, consistent with interconnection concepts already studied in

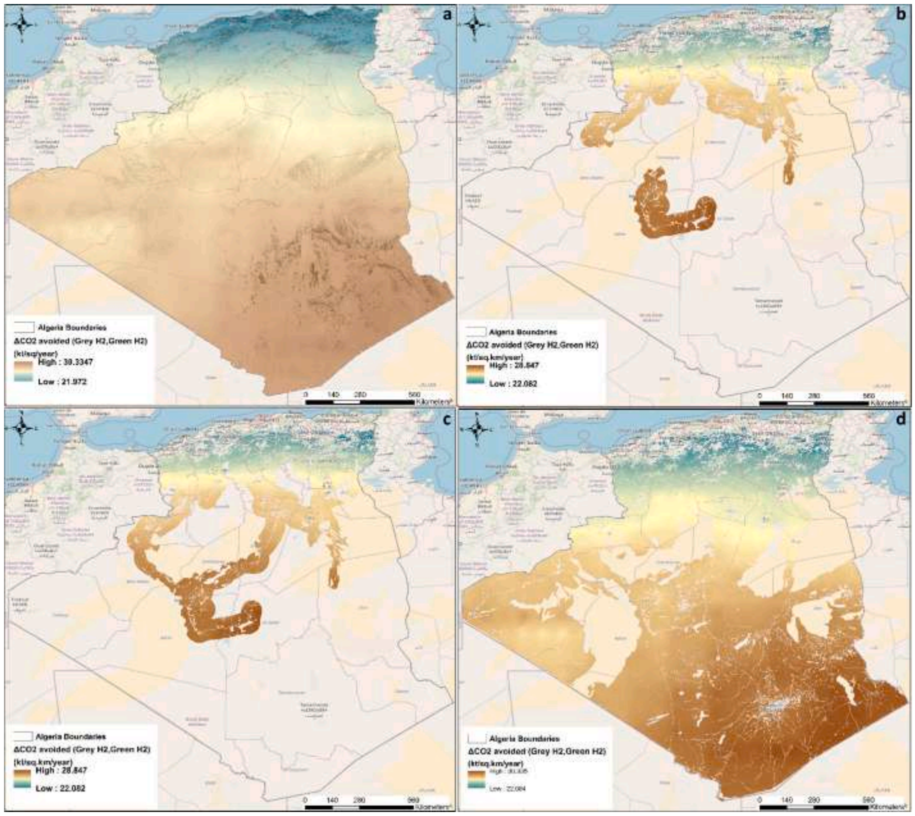

Fig. 14. Spatial distribution of avoided CO_2 emissions relative to grey hydrogen for Horizontal PV-driven hydrogen production across Algeria under grid-availability scenarios (a) baseline (unconstrained), (b) on-grid eligible areas, (c) on-grid North–South (N—S) interconnection corridor, and (d) off-grid eligible scenario. Units (kt $CO_2 \cdot km^{-2} \cdot yr^{-1}$).

regional transmission planning.

In particular, Med TSO describes an exploratory Algeria–Italy (Sardinia) HVDC interconnection (Cheffia–Cagliari Sud) with a nominal capacity of 1000 MW and an approximate length of ~350 km, and frames it as a long term option within its regional planning outlook. Complementing this planning context, a 2024 MoU indicates renewed institutional interest in assessing an Algeria–Europe subsea electricity link [72].

The three scenarios presented here are intended as export pathway concepts derived from the spatial atlas evidence base, rather than bankable engineering designs. A full comparison requires additional technical and economic analysis that is outside the scope of this screening study. In particular, because PV generation is temporally variable, matching production to export delivery profiles would require system flexibility (e.g., hydrogen buffer storage, line pack and/or conversion to carriers, PV overbuild with controlled curtailment, and flexible Electrolyzer operation) to enable stable export and contract-aligned delivery.

For Scenario 1, this includes sizing the PV supply (or certified electricity procurement) required to support groundwater pumping, conveyance, and treatment; quantifying hydrogen pipeline energy requirements (compression, boosting, and potential recompression stations) from the inland production areas to export interfaces; and translating these auxiliary loads into delivered cost impacts and land requirements for additional PV capacity. Given Algeria's existing gas transport and export corridors, pipeline-based export concepts may offer an advantageous starting point for large-volume delivery, but repurposing/parallel construction, permitting, and compressor station requirements must be assessed in a dedicated corridor-level design study.

For Scenario 2, the desalination integrated configuration is based on an existing coastal plant capacity and does not yet include an economic allocation of desalinated water, a detailed polishing train to Electrolyzer specifications, or the dedicated renewable power plant sizing needed to supply desalination and electrolysis under clean electricity constraints. For Scenario 3, the electricity export option similarly requires explicit HVDC and grid reinforcement cost modelling, losses, and certification boundary conditions. Across all scenarios, achieving a 10 Mt. $H_2 \cdot yr^{-1}$ export scale implies staged build-out of PV, Electrolyser, and transport infrastructure; here it is treated as a policy-relevant reference scale for screening rather than a deployment schedule. These follow on assessments are essential to identify the most robust pathway for export scale deployment and will be addressed in future work.

While the results indicate strong resource-based potential for export-oriented hydrogen production, practical deployment at large scale will also depend on how temporal variability in PV generation is managed, for example through flexible Electrolyze operation and intermediate hydrogen storage. In addition, scaling from site-level potential to export-relevant volumes would require phased expansion of transport, storage, water-supply, and port-related infrastructure. These aspects constitute important feasibility constraints beyond the present spatial techno-economic scope and warrant dedicated system-integration analysis in future work.

9. Generalizability and transferability

While this study applies the framework to Algeria, most methodological components are transferable, including PV performance modelling, PV–electrolysis coupling and sizing, spatial LCOH mapping, scenario masking to represent infrastructure/policy constraints, and screening indicators derived from the land-normalized hydrogen output atlas.

By contrast, several aspects of the *results* are context-dependent. Algeria-specific drivers include the availability of large contiguous desert land, the existing grid footprint and corridor logic used to

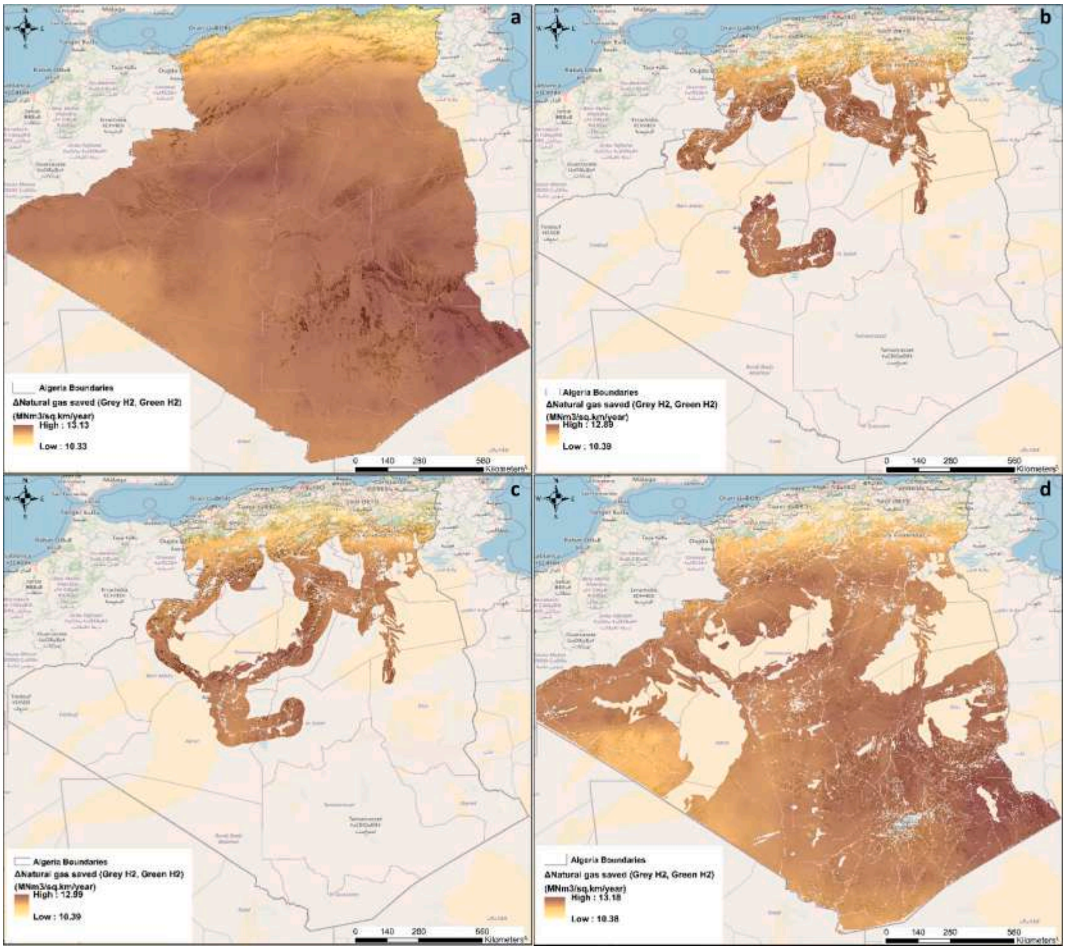

Fig. 15. Spatial distribution of **natural gas saved** relative to grey hydrogen for Tilted PV-driven hydrogen production across Algeria under grid-availability scenarios (a) baseline (unconstrained), (b) on-grid eligible areas, (c) on-grid North–South (N—S) interconnection corridor, and (d) off-grid eligible scenario. Units **($MNm^3 \cdot km^{-2} \cdot yr^{-1}$).**

represent feasible connection, and water-supply constraints motivating groundwater and desalination-linked variants. These factors largely determine how much of the resource-driven low-cost envelope becomes practically realizable.

The main insights generalize well to other high-solar, export-oriented settings in Africa/MENA with extensive arid land and high irradiation, where CAPEX-dominated economics reward high annual hydrogen yield and infrastructure access governs feasibility. Transferability is less direct for densely populated, lower-solar contexts (typical of many European regions), where land competition and weaker solar resource shift the solution space toward alternative siting and supply options (e.g., offshore wind, stronger reliance on grid electricity, or imported hydrogen/e-fuels).

10. Conclusion

This work developed a territory wide, scenario conditioned screening framework for green hydrogen deployment in Algeria by coupling a **PV DC yield atlas** (horizontal and optimally tilted) with spatial conversion to **hydrogen production density, LCOH**, and screening level **environmental co benefits** relative to grey hydrogen. By expressing PV output on a land normalized DC basis and applying four feasibility scenarios unconstrained, grid eligible, North–South corridor, and off grid the analysis distinguishes clearly between *technical potential* and *deployable potential* as constrained by infrastructure availability.

Across Algeria, the PV to hydrogen chain exhibits a coherent spatial structure areas with higher PV DC yield translate directly into higher hydrogen production density and lower LCOH, which then determine the magnitude and spatial concentration of avoided emissions and displaced natural gas. Incorporating optimal tilt consistently improves performance relative to horizontal PV, confirming that tilt optimization acts not only as an energy yield enhancement but also as an economic lever that strengthens competitiveness across the mapped domain. Under the adopted techno economic assumptions, LCOH remains within **~4.6–5.2 €/kg H_2,** and the lowest cost regions align with the highest PV to H_2 productivity. A targeted sensitivity analysis at the best-performing location shows that absolute costs are dominated by PV and Electrolyzer capital costs and financing conditions: across the explored parameter space, best-site LCOH spans ~2.27–7.62 €/kg H_2, with monotonic increases under higher CAPEX and discount rates, while realistic Electrolyser-efficiency improvements yield comparatively smaller reductions.

Infrastructure availability strongly conditions where competitive hydrogen is *practically* realizable. Grid eligibility constraints concentrate feasible production into the existing northern grid footprint, potentially excluding parts of the interior resource advantaged zones. The proposed North–South interconnection corridor expands access to interior areas and increases the reachable share of lower LCOH regions compared with a strict grid only strategy. The off grid scenario recovers much of the technical low cost envelope, highlighting that, once grid constraints are relaxed, non-resource factors (water supply, logistics, and hydrogen transport/export infrastructure) become decisive for bankability.

For export scale illustration, the atlas derived mean hydrogen

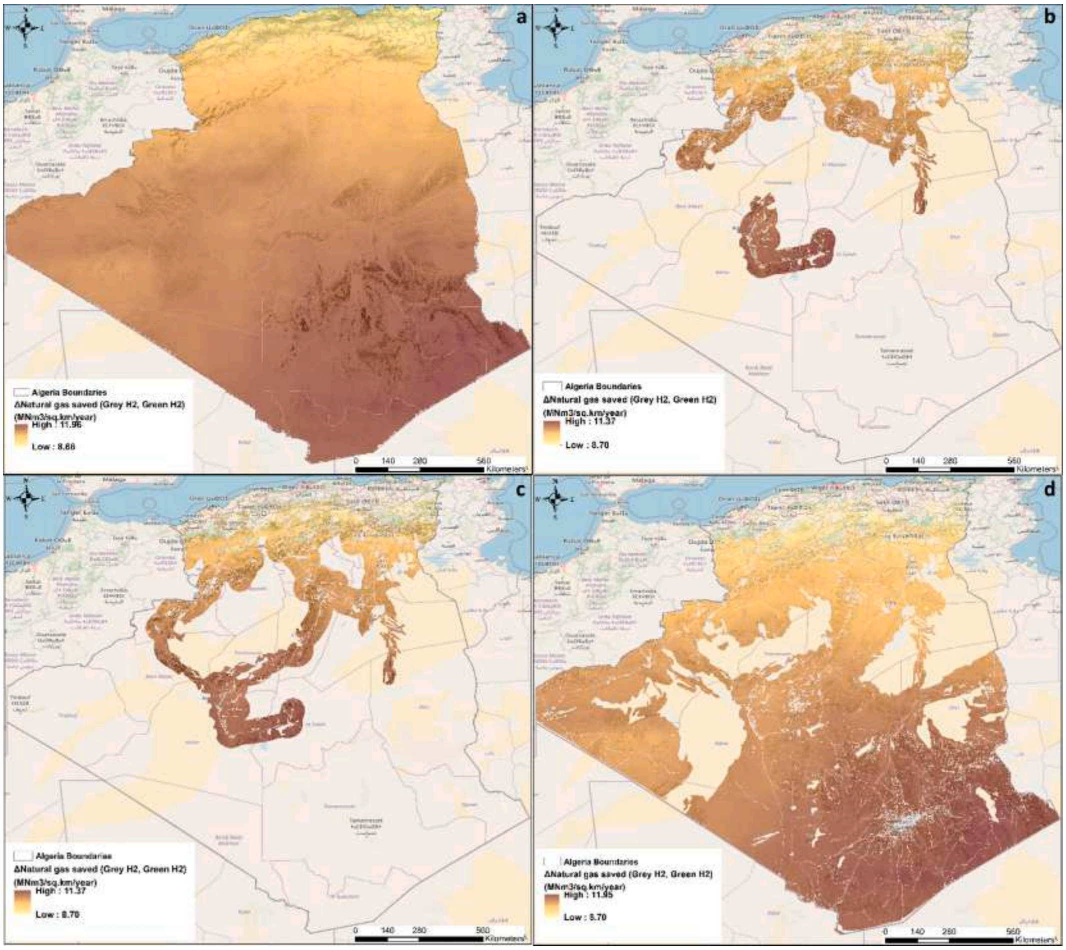

Fig. 16. Spatial distribution of **natural gas saved** relative to grey hydrogen for Horizontal PV-driven hydrogen production across Algeria under grid-availability scenarios (a) baseline (unconstrained), (b) on-grid eligible areas, (c) on-grid North–South (N–S) interconnection corridor, and (d) off-grid eligible scenario. Units **($MNm^3 \cdot km^{-2} \cdot yr^{-1}$)**.

production intensities imply that achieving **10 Mt $H_2 \cdot yr^{-1}$** would require on the order of **~3714 km^2 in Ain Salah (southern Algeria)** and **~ 3784 km^2 in Laghouat (north central Algeria),** based on the highlighted provincial mean production densities **(2692.21** and **2642.68 $t \cdot km^{-2} \cdot yr^{-1}$,** respectively). At the stoichiometric requirement of **9 L/kg H_2,** producing **10 Mt $H_2 \cdot yr^{-1}$** implies a minimum consumptive feedwater demand of **~90,000,000 $m^3 \cdot yr^{-1}$.** If supplied by treated desalinated water, a coastal desalination facility rated at **300,000 $m^3 \cdot day^{-1}$** could provide approximately **109,500,000 $m^3 \cdot yr^{-1}$,** sufficient to cover the stoichiometric feedwater for 10 Mt.$\cdot yr^{-1}$ (with margin), subject to project specific losses and water quality requirements. Ensuring the hydrogen qualifies as green additionally requires that electricity supplied to electrolysis and any desalination process be matched with certified renewable generation, rather than mixed grid power.

Overall, the combined atlases and scenario filters provide a transparent basis for prioritizing hydrogen zones, comparing horizontal versus tilted PV pathways, and understanding how grid strategies influence the realizable volume of low cost hydrogen. Future work should extend the present screening into delivery cost optimization (pipelines vs. carriers vs. electricity export), explicit water system constraints (local hydrogeology, abstraction limits, and treatment energy), and higher resolution operational matching between PV generation and Electrolyzer utilization.

Declaration of generative AI and AI assisted technologies in the writing process

During the preparation of this manuscript, the authors used ChatGPT only as a language editing tool, for grammar checking and occasional improvement of sentence clarity. All content was subsequently reviewed and revised by the authors, who accept full responsibility for the final text of the publication.

CRediT authorship contribution statement

Mawloud Guermoui: Writing – review & editing, Writing – original draft, Visualization, Validation, Software, Resources, Methodology, Investigation, Formal analysis, Data curation. **Abdelfetah Belaid:** Formal analysis, Data curation. **Farid Melgani:** Writing – review & editing, Visualization, Validation, Supervision, Methodology, Investigation, Formal analysis, Conceptualization.

Declaration of competing interest

The authors declare that they have no known competing financial interests or personal relationships that could have appeared to influence the work reported in this paper.

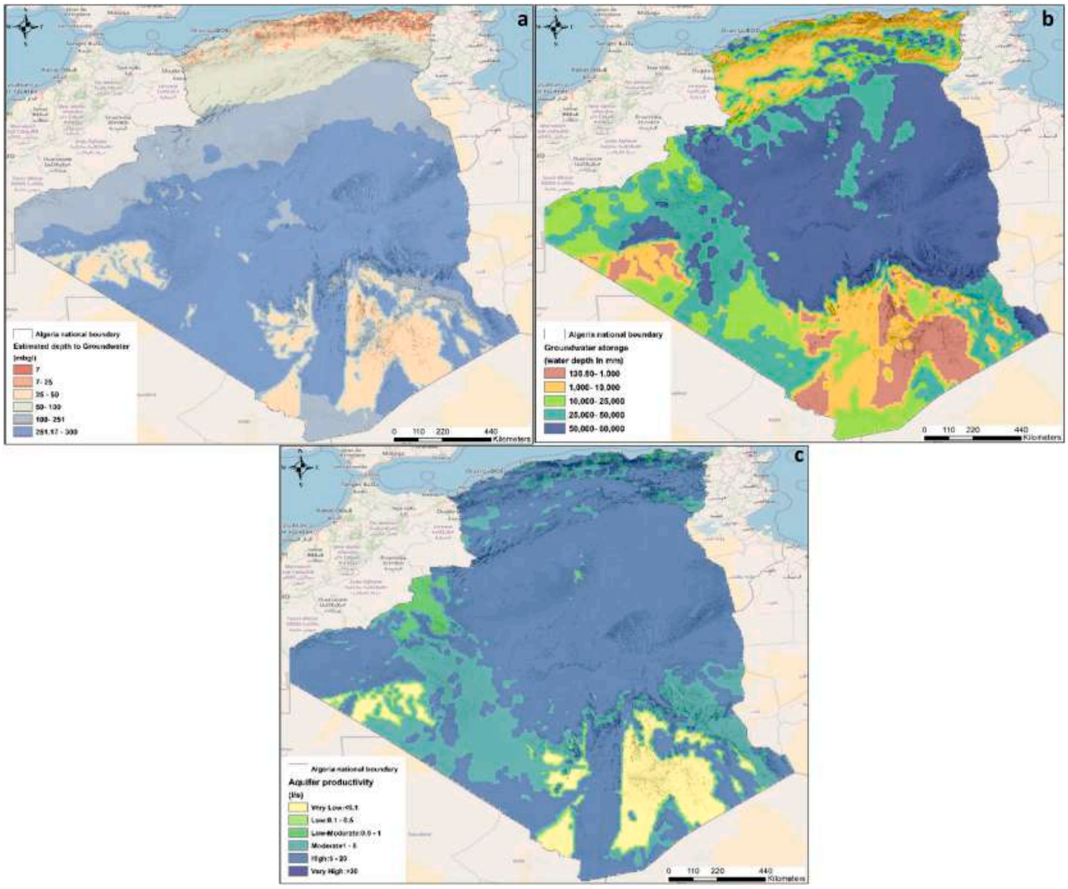

Fig. 17. Groundwater characteristics across Algeria a) depth to water table, b) groundwater storage, and c) aquifer productivity.

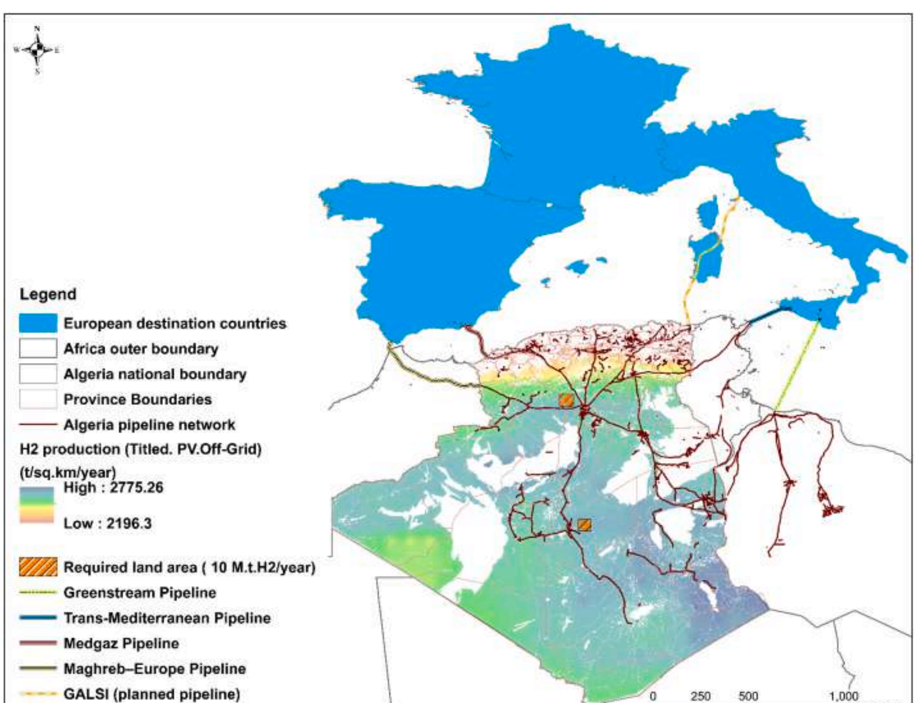

Fig. 18. Spatial overlay of off-grid PV–H_2 production potential, required land area (10 Mt. $H_2 \cdot yr^{-1}$), and Algeria–Europe pipeline corridors.

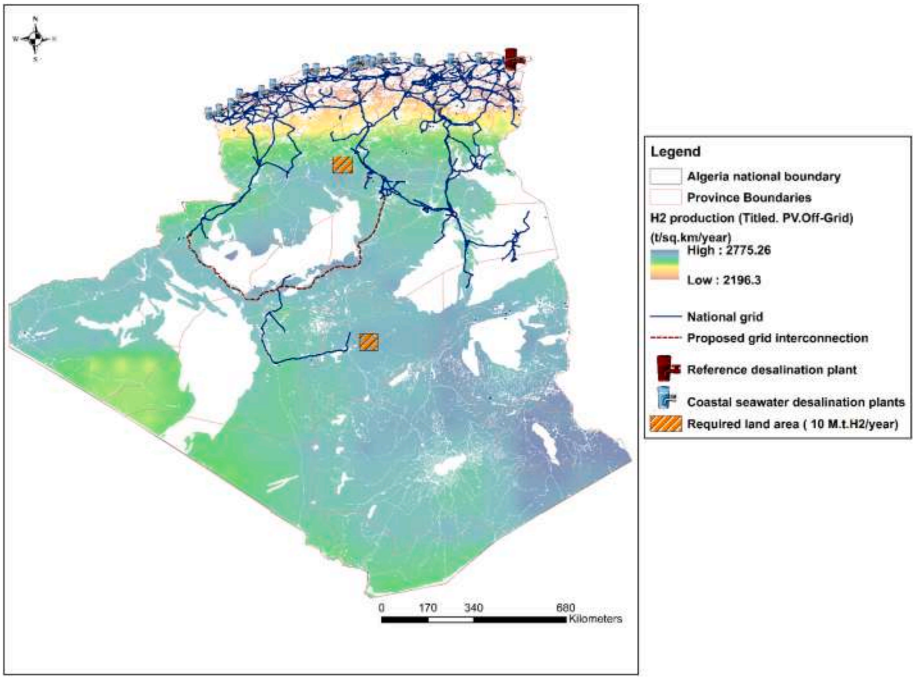

Fig. 19. Desalination-supported green hydrogen, land footprint and proposed grid interconnection. (For interpretation of the references to colour in this figure legend, the reader is referred to the web version of this article.)

Acknowledgement

This work is supported by the EU Horizon Europe MSCA Postdoctoral Fellowship RESSAIG, Grant Agreement No. 101197884.Funded by the European Union. Views and opinions expressed are however those of the author(s) only and do not necessarily reflect those of the European Union or The European Research Executive Agency. Neither the European Union nor the granting authority can be held responsible for them.

Appendix A. Appendix A reports the input parameters used for PV DC yield modelling, PV to hydrogen conversion, and LCOH. Calculations are performed on the DC side at the Electrolyzer input (including DC/DC losses where applicable) and hydrogen is reported on an HHV basis. LCOH includes PV and Electrolyzer CAPEX (plus indirect adder), fixed O&M, and stack replacement costs as specified in Table A1

Table A1
Key input parameters and techno economic assumptions used for PV–H_2 modelling and LCOH calculation.

Parameter	Symbol	Value	Unit	Ref
Electrolyzer operating hours per day	n	7.5	$h \cdot day^{-1}$	–
Electrolyzer annual operating hours	H_{EZ}	$n \times 365 = 2737.5$	$h \cdot yr^{-1}$	–
Electrolyzer rated power	P_{EZ}	50,000	kW	–
DC/DC efficiency (DC coupled)	η_{dc}	0.95	–	–
PV module (Sandia database entry)	–	SunPower_SPR_220_BLK_U_Module_2008_E_	–	–
Electrolyzer efficiency (HHV basis)	η_{EZ}	0.7723	–	[73,74]
Hydrogen HHV	HHV_{H2}	39.39	$kWh \cdot kg^{-1}$	[73,74]
Discount rate	r	0.06	–	[73]
Overhead / indirect cost adder	ϕ	0.19	–	[73]
PV CAPEX	$CAPEX_{PV}$	900	€/kW	[73]
Electrolyzer CAPEX	$CAPEX_{EZ}$	1000	€/kW	[73]
PV fixed O&M fraction	f_{PV}	0.018	yr^{-1}	[73]
Electrolyzer fixed O&M fraction	f_{EZ}	0.019	yr^{-1}	[73,74]
Stack replacement fraction of Electrolyzer CAPEX	γ	0.45	–	[73]

Appendix B. Transmission grid and proposed north–south interconnection

The existing transmission network shown in Fig. B1 represents the currently operational high-voltage grid (as available in the referenced dataset). The proposed north–south interconnection (dashed line) is included as a planning assumption to test the effect of improved inland connectivity between the northern load centers and the southern regions with high solar resource potential. This proposed corridor is used only for scenario evaluation and does not represent a committed construction plan unless stated in the reference source.

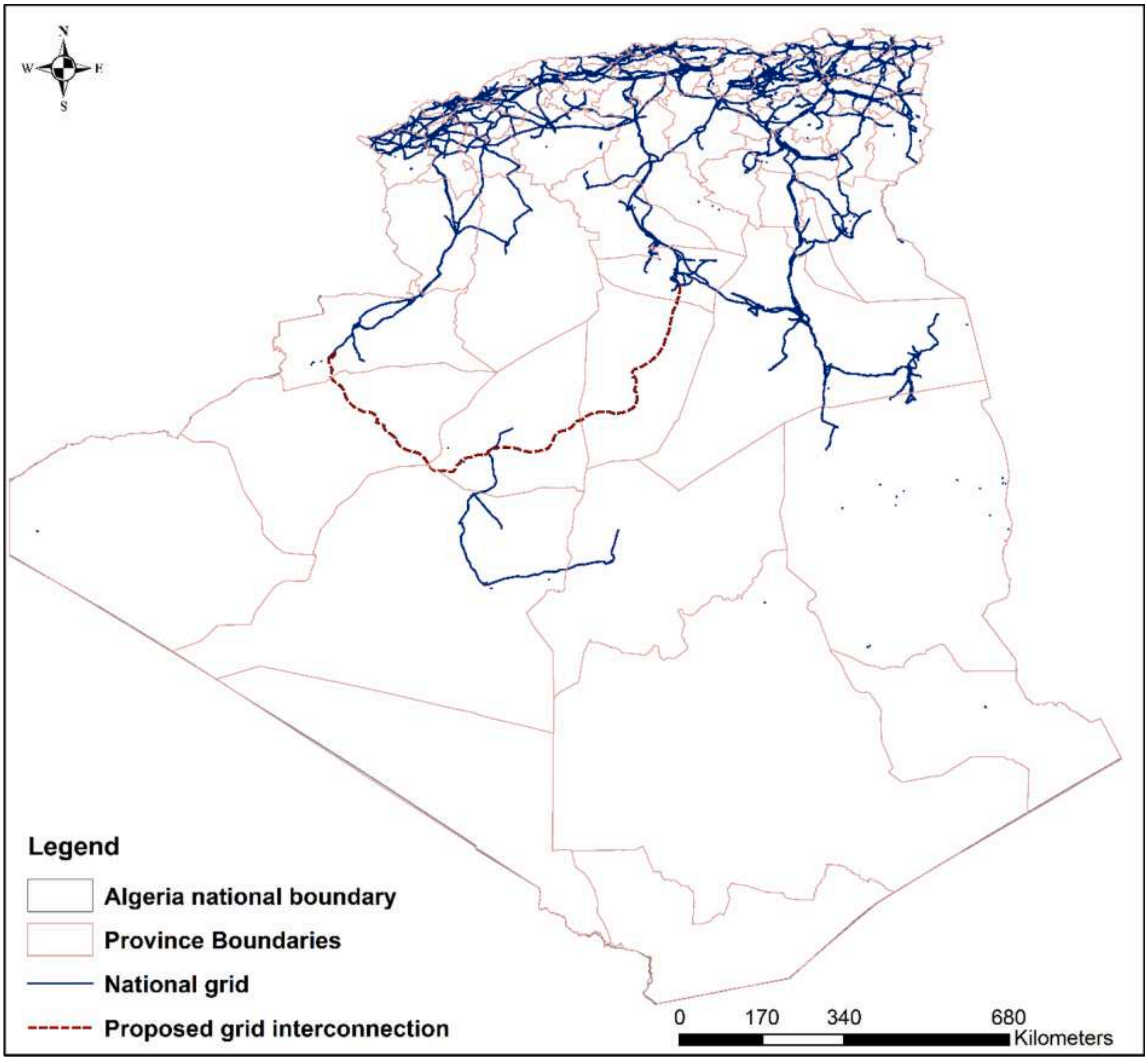

Fig. B1. Existing high-voltage electricity transmission grid in Algeria and the proposed north–south interconnection corridor considered in this study. Provincial boundaries are shown for geographic reference.

Data availability

Data will be made available on request.

References

[1] De Almeida JO, Shadman M, dos Santos Ramos J, Bastos ITC, Silva C, Chujutalli JAH, et al. Techno economic analysis of hydrogen production from offshore wind the case of Brazil. Energy Convers Manag 2024;322:119109. https://doi.org/10.1016/j.enconman.2024.119109.

[2] Hydrogen Council. Hydrogen for Net Zero A critical cost competitive energy vector. Nov. 2021. Accessed Dec. 27. 2025 [Online]. Available https //hydrogencouncil.com/wp content/uploads/2021/11/Hydrogen for Net Zero.pdf.

[3] Li X, Tang X, Ma M, Wang M, Xu C. Levelized cost analysis of onshore wind powered hydrogen production system in China considering landform heterogeneity. Energy 2024;313:133942. https://doi.org/10.1016/j.energy.2024.133942.

[4] Kadam RS, Sutar PR, Yadav GD. Energy and environmental assessment of industrial scale hydrogen production comparison of steam methane reforming, electrolysis, and cu–cl cycles. Int J Hydrog Energy 2025;106(994):1005. https://doi.org/10.1016/j.ijhydene.2025.01.439.

[5] de Azevedo JHP, Pradelle F, Botelho V, Serra ET, Pradelle RNC, Braga SL. An integrated geospatial model for evaluating offshore wind to hydrogen technical and economic production potential in Brazil. Int J Hydrog Energy 2025;100(800):815. https://doi.org/10.1016/j.ijhydene.2024.12.333.

[6] International Energy Agency (IEA). Global Hydrogen Review 2025. Paris, France: IEA. Accessed: Feb. 23, 2026. [Online]. Available: https://iea.blob.core.windows.net/assets/12d92ecc-e960-40f3-aff5-b2de6690ab6b/GlobalHydrogenReview2025.pdf; 2025.

[7] International Energy Agency (IEA). "GHG emissions of hydrogen and its derivatives," *Global Hydrogen Review* 2024. 2024. Accessed Dec. 27, 2025. [Online]. Available https //www.iea.org/reports/global hydrogen review 2024/ghg emissions of hydrogen and its derivatives.

[8] UNFCCC. "The Kyoto Protocol," *UNFCCC*. 2025 [Online]. [Available https //unfccc.int/process and meetings/the kyoto protocol].

[9] UNFCCC. "The Paris Agreement," *UNFCCC*. 2025 [Online]. [Available https //unfccc.int/process and meetings/the paris agreement].

[10] Halimi Y, Halimi S, Bouzid Z, Ghellai N. Spatially-optimized photovoltaic site selection in Algeria: assessing solar potential using high-resolution data, GIS, and multicriteria analysis. Energy Convers Manag 2025;323:119176. https://doi.org/10.1016/j.enconman.2024.119176.

[11] SGS INSPIRE. "Algeria National strategy for hydrogen development published." Feb. 2024. Accessed Dec. 27. 2025 [Online]. Available https //inspire.sgs.com/content/101104598/algeria national strategy for hydrogen development published.

[12] European External Action Service (EEAS). Delegation of the European Union to Algeria, "Lancement de la phase cofinancée par l'UE et l'Allemagne du projet « TaqatHy+ »." Apr. 15, 2025. Accessed Dec. 27. 2025 [Online]. Available https //www.eeas.europa.eu/delegations/algeria/lancement de la phase cofinanc%C3%A9e par l%E2%80%99ue et l%E2%80%99allemagne du projet %C2%AB taqathy %C2%BB_fr?s=82.

[13] European Commission. REPowerEU Plan (Communication), COM(2022) 230 final, May 18, 2022. Accessed Dec. 28. 2025 [Online]. Available https //eur lex.europa.eu/legal content/EN/TXT/?uri=CELEX 52022DC0230.

[14] European Commission. Communication on the European Hydrogen Bank, COM (2023) 156 final, Mar. 16. 2023. Accessed Dec. 28, 2025. [Online]. Available https //eur lex.europa.eu/legal content/EN/TXT/PDF/?uri=CELEX 52023DC0156.

[15] Solano Edna S, Affonso Carolina M. Wind and solar-based green hydrogen potential in Brazil: production, costs, and CO2 mitigations. Int J Hydrog Energy 2025;172:151212. https://doi.org/10.1016/j.ijhydene.2025.151212.

[16] Nasser Mohamed, Hassan Hamdy. Feasibility analysis and atlas for green hydrogen project in MENA region: production, cost, and environmental maps. Sol Energy 2024;268:112326. https://doi.org/10.1016/j.solener.2024.112326.

[17] Nasser Mohamed, Hassan Hamdy. Egyptian green hydrogen atlas based on available wind/solar energies: power, hydrogen production, cost, and CO2 mitigation maps. Int J Hydrog Energy 2024;50:487–501. https://doi.org/10.1016/j.ijhydene.2023.09.127.

[18] Attiaoui Mohammed, et al. Techno-economic and GIS mapping of wind-driven hydrogen production in Portugal. Int J Hydrog Energy 2025;151:150157. https://doi.org/10.1016/j.ijhydene.2025.150157.

[19] Jiménez Andrea Navarro. Mapping China's green hydrogen: provincial LCOH, resource endowments, and policy pathways. Fuel 2026;405:136326. https://doi.org/10.1016/j.fuel.2025.136326.

[20] Li Yinan, et al. Scaling solar photocatalytic hydrogen production in China: integrated geospatial-meteorological analysis. Appl Energy 2025;381:125179. https://doi.org/10.1016/j.apenergy.2024.125179.

[21] Taoufik, FEKRI Meryem, Ahmed. A GIS-based multi-criteria decision-making approach for site suitability analysis of solar-powered hydrogen production in the Souss-Massa region, Morocco. Renewable Energy Focus 2023;46:385–401. https://doi.org/10.1016/j.ref.2023.08.004.

[22] FLORA, Fotsing Metegam Isabelle.. A GIS-based on application of Monte Carlo and multi-criteria decision-making approach for site suitability analysis of solar-hydrogen production: case of Cameroon. Heliyon 2025;11, no 1. https://doi.org/10.1016/j.heliyon.2024.e41541.

[23] FLORA, Fotsing Metegam Isabelle.. An MCDM-GIS based site suitability analysis for solar power plant integration in Cameroon: solar hybridization to optimize green electricity and hydrogen production. Int J Hydrog Energy 2025;106:23–51. https://doi.org/10.1016/j.ijhydene.2025.01.445.

[24] Kihel EL, Badr et ELYAMANI, Nacer Eddine El Kadri.. Original approach to the techno-economic optimization of wind-based electricity and green hydrogen production: integrating Weibull analysis with multi-criteria decision-making. Results. Engineering 2025:108397. https://doi.org/10.1016/j.rineng.2025.108397.

[25] Rouzbahani Fatemeh, Rad Mohammad Amin Vaziri, Aghajani Danyal. Mapping cost-effective hydrogen production based on renewable resource potential and techno-economic analysis: a case study. Appl Energy 2026;404:127160. https://doi.org/10.1016/j.apenergy.2025.127160 10.

[26] Omid Nematollahi, Pouria Alamdari, Mehdi Jahangiri, et al. A techno-economical assessment of solar/wind resources and hydrogen production: A case study with GIS maps. Energy 2019;175:914–30. https://doi.org/10.1016/j.energy.2019.03.125.

[27] İzgeç MM, Emre T. Strategic siting and cost modeling for green hydrogen export from off-grid renewables: A multi-hub approach for Türkiye. Int J Hydrog Energy 2026;210:153616. https://doi.org/10.1016/j.ijhydene.2026.153616.

[28] Xinying Cai, Nan Zhang, Du-Ikonen Liuliu, et al. Design a nationwide hydrogen grid: A GIS-based and iterative optimization model integrating pathfinding and dispatch. Int J Hydrog Energy 2025;154:150253. https://doi.org/10.1016/j.ijhydene.2025.150253.

[29] da Silveira Cachola, Celso, and Drielli Peyerl.. Mapping green hydrogen clusters in Brazil: A data-driven approach for industrial decarbonization. Int J Hydrog Energy 2026;206:153202. https://doi.org/10.1016/j.ijhydene.2025.153202.

[30] Odhiambo Joab Onyango, et al. "pathways to green hydrogen production as a sustainable energy solution in Kenya by 2040." discover. Energy 2025;5(1):37. https://doi.org/10.1007/s43937-025-00098-0.

[31] Khasawneh Hussam J, Maaitah Rawan A, AlShdaifat Ahmad. Green hydrogen in Jordan: stakeholder perspectives on technological, infrastructure, and economic barriers. Energies 2025;18(15):3929. https://doi.org/10.3390/en18153929.

[32] Soumia Rahmouni, Belkhir Negrou, Noureddine Settou, et al. Prospects of hydrogen production potential from renewable resources in Algeria. Int J Hydrog Energy 2017;42(2):1383–95. https://doi.org/10.1016/j.ijhydene.2016.07.214.

[33] Mraoui, A. et Menia, S.. Renewable electrolytic hydrogen potential in Algeria. Int J Hydrog Energy 2019;44(49):26863–73. https://doi.org/10.1016/j.ijhydene.2019.08.134.

[34] Mohamed Blal, Ahmed Belasri, Ali Benatillah, et al. Assessment of solar and wind energy as motive for potential hydrogen production of Algeria country; development a methodology for uses hydrogen-based fuel cells. Int J Hydrog Energy 2018;43(19):9192–210. https://doi.org/10.1016/j.ijhydene.2018.03.200.

[35] MESSAOUDI, Djilali, SETTOU, Noureddine, et ALLOUHI, Amine.. Geographical, technical, economic, and environmental potential for wind to hydrogen production in Algeria: GIS-based approach. Int J Hydrog Energy 2024;50:142–60. https://doi.org/10.1016/j.ijhydene.2023.07.263.

[36] Guermoui M, Melgani F, Danilo C. Multi step ahead forecasting of daily global and direct solar radiation a review and case study of Ghardaia region. J Clean Prod 2018;201(716):734. https://doi.org/10.1016/j.jclepro.2018.08.006.

[37] Guermoui M, Fezzani A, Mohamed Z, Rabehi A, Ferkous K, Bailek N, et al. An analysis of case studies for advancing photovoltaic power forecasting through multi scale fusion techniques. Sci Rep 2024;14(1):6653. https://doi.org/10.1038/s41598 024 57398 z.

[38] Kremia W. Sonelgaz, Pilote de la transition énergétique en Algérie (Communication n°4). Club Energy (Association Nationale "Club Energy"), March [Online]. Available: https://clubenergy-dz.com/wp-content/uploads/2025/03/8-Communication-n%C2%B04-par-W.-Kremia.pdf; 2025. accessed Feb. 24, 2026.

[39] Aux Commissariat. Énergies Renouvelables et à l'Efficacité Énergétique (CEREFE). Bilan des secteurs jusqu'à fin 2023. Algiers, Algeria: CEREFE. Available at: https://www.cerefe.gov.dz/storage/138/Bilan-des-secteurs-jusqua-fin-2023_.pdf; 2024.

[40] Milbrandt A, Mann M. Potential for hydrogen production from key renewable resources in the United States (Technical Report No. NREL/TP 640 41134). National Renewable Energy Laboratory. 2007. https://doi.org/10.2172/899141.

[41] Elkadeem Mohamed R, et al. A spatio temporal decision making model for solar, wind, and hybrid systems–A case study of Saudi Arabia. Appl Energy 2025;383:125277. https://doi.org/10.1016/j.apenergy.2025.125277.

[42] Yilmaz İsmail, Kocer Abdulkadir, Aksoy Ercument. Site selection for solar power plants using GIS and fuzzy analytic hierarchy process case study of the western mediterranean region of Turkiye. Renew Energy 2024;237:121799. https://doi.org/10.1016/j.renene.2024.121799.

[43] Rios R, Duarte S. Selection of ideal sites for the development of large scale solar photovoltaic projects through Analytical Hierarchical Process–Geographic information systems (AHP GIS) in Peru. Renew Sust Energ Rev 2021;149:111310. https://doi.org/10.1016/j.rser.2021.111310.

[44] Shahid ALI, et al. GIS based site suitability assessment for wind and solar farms in Songkhla, Thailand. Renew Energy 2019;132(1360):1372. https://doi.org/10.1016/j.renene.2018.09.035.

[45] Merrouni Ahmed Alami, et al. Large scale PV sites selection by combining GIS and analytical hierarchy process. Case study eastern Morocco. Renew Energy 2018;119(863):873. https://doi.org/10.1016/j.renene.2017.10.044.

[46] Garni AL, Hassan Z, Anjali Awasthi. Solar PV power plants site selection A review. Advances in renewable energies and power technologies. 2018. 57 75. Doi: 10.1016/B978 0 12 812959 3.00002 2.

[47] Q Wang, L PohK. A survey of integrated decision analysis in energy and environmental modeling. Energy 2014;77(691):702. https://doi.org/10.1016/j.energy.2014.09.060.

[48] Abbas Mardani, et al. Sustainable and renewable energy an overview of the application of multiple criteria decision making techniques and approaches. Sustainability 2015. https://doi.org/10.3390/su71013947. 7.10 13947 13984.

[49] Ghasemi Golara, et al. Theoretical and technical potential evaluation of solar power generation in Iran. Renew Energy 2019;138. https://doi.org/10.1016/j.renene.2019.02.068. 1250 1261.

[50] Rekik Sassi, El Alimi Souheil. Optimal wind solar site selection using a GIS AHP based approach a case of Tunisia. Energy Convers Manag 2023;*X* 18:100355. https://doi.org/10.1016/j.ecmx.2023.100355.

[51] Metegam Isabelle Flora, Fotsing, et al. Evaluation of on grid and off grid solar photovoltaic sites in Cameroon using geographic information systems, fuzzy logic, and multi criteria analysis. Energy 2025;318:134614. https://doi.org/10.1016/j.energy.2025.134614.

[52] Perez Richard, et al. Modeling daylight availability and irradiance components from direct and global irradiance. Sol Energy 1990;44(5). 271 289. Doi: 10.1016/0038 092X(90)90055 H.

[53] King DL, Boyson WE, Kratochvil JA. Photovoltaic array performance model. Albuquerque, NM, USA: Sandia National Laboratories; 2004. Tech. Rep. SAND2004 3535,.

[54] Lappalainen K, Manganiello P, Piliougine M, Spagnuolo G, Valkealahti S. Virtual sensing of photovoltaic module operating parameters. IEEE J Photovoltaics 2020;10(3):852–62. https://doi.org/10.1109/JPHOTOV.2020.2972688.

[55] Loukarfi L, Boudjelthia RE, Khelfaoui A, Belhadj A. Assessment of rooftop solar photovoltaic potential in Algeria using a new geospatial methodology. Renew Energy 2023;201:787–805.

[56] Ishaque Y, Shafiullah M, Al Ahmed AA. "Hydrogen production assessment using curtailed electricity of firm PV power plants A case study of Saudi Arabia," Energy Conversion and Managementvol. 315; 2024. Art [no. 118754].

[57] Saif AGH, Alquaity AB, Mokheimer EM. Techno economic analysis of green hydrogen production in Saudi Arabia A comparative study of solar PV and CSP technologies. Int J Hydrog Energy 2025;105(1361):1374. https://doi.org/10.1016/j.ijhydene.2025.01.043.

[58] Nasser M, Hassan H. Egyptian green hydrogen atlas based on available wind/solar energies power, hydrogen production, cost, and CO2 mitigation maps. Int J Hydrog Energy 2024;50(487):501. https://doi.org/10.1016/j.ijhydene.2023.09.127.

[59] International Energy Agency. Towards hydrogen definitions based on their emissions intensity. Paris, France IEA. 2023.

[60] Connelly D, Elgowainy A, Reddi K. *Resource assessment for hydrogen production* (NREL/TP 5400 77198). Golden, CO National Renewable Energy Laboratory; 2020.

[61] Tahir MM, Abbas A, Dickson R. Green hydrogen and chemical production from solar energy in Pakistan A geospatial, techno economic, and environmental assessment. Int J Hydrog Energy 2025;116(613):626. https://doi.org/10.1016/j.ijhydene.2025.03.067.

[62] Soufiane B. Integrated geospatial and techno economic analysis of green hydrogen generation from offshore wind A case study of Morocco. Int J Hydrog Energy 2026;207. https://doi.org/10.1016/j.ijhydene.2026.153490.

[63] Al Ghussain L, Lu Z, Alrbai M, Al Dahidi S, He X, Elgowainy A, et al. Global techno economic and life cycle greenhouse gas emissions assessment of solar and wind based renewable hydrogen production. Appl Energy 2025;401:126595. https://doi.org/10.1016/j.apenergy.2025.126595.

[64] Khatri SA, Harijan K, Uqaili MA, Shah SF, Mirjat NH, Kumar L. Solar photovoltaic potential and diffusion assessment for Pakistan. Energy Sci Eng 2022;10(7):2452 2474. https://doi.org/10.1002/ese3.1149.
[65] International Renewable Energy Agency (IRENA). Renewable Power Generation Costs in 2023. Abu Dhabi, UAE IRENA. 2024. ISBN 978 92 9260 593 3.
[66] International Energy Agency (IEA). Global hydrogen review 2025 revised version. Paris, France IEA 2025:2025.
[67] Palmer G, Roberts A, Hoadley A, Dargaville R, Honnery D. Life-cycle greenhouse gas emissions and net energy assessment of large-scale hydrogen production via electrolysis and solar PV. Energy Environ Sci 2021;14:5113–31. https://doi.org/10.1039/D1EE01288F.
[68] European Hydrogen Backbone (EHB). A European hydrogen infrastructure vision covering 28 countries.Guidehouse; EHB initiative. Available *at*, https://www.ehb.eu/files/downloads/EHB-A-European-hydrogen-infrastructure-vision-covering-28-countries.pdf; 2022. accessed 22 Feb 2026.
[69] Guillot V, Assoumou E. Power and green hydrogen trade potential between north African and European countries: conditions, challenges, and sustainability prospects. Appl Energy 2024. https://doi.org/10.1016/j.apenergy.2024.125209.
[70] Beswick RR, Oliveira AM, Yan Y. Does the green hydrogen economy have a water problem? ACS Energy Lett 2021;6(9). https://doi.org/10.1021/acsenergylett.1c01375. 3167 3169.
[71] Tonelli D, Rosa L, Gabrielli P, Caldeira K, Parente A, Contino F. Global land and water limits to electrolytic hydrogen production using wind and solar resources. Nat Commun 2023;14(1):5532. Doi: 10.1038/s41467 023 41107 x.
[72] Reuters. “Algeria’s oil and gas firms sign MoU with Eni for electricity supply, Sonatrach says.” 31 Jul 2024. Accessed 25 Oct. 2025.
[73] Fraunhofer ISI, Fraunhofer ISE. Assessment and analysis of the power to X market and investment opportunities in Algeria. Germany: Final report; 2024.
[74] Wolf N, Neuber R, Mädlow A, Höck M. Techno economic analysis of green hydrogen supply for a hydrogen refueling station in Germany. Int J Hydrog Energy 2025;106(318):333. https://doi.org/10.1016/j.ijhydene.2025.01.424.